THE ASTROPHYSICAL JOURNAL, 344:805–825, 1989 September 15

A DETAILED STUDY OF THE REMNANT OF NOVA GK PERSEI AND ITS ENVIRONS

E. R. SEAQUIST,[1] M. F. BODE,[2] D. A. FRAIL,[1] J. A. ROBERTS,[2] A. EVANS,[3] AND J. S. ALBINSON[3]

Received 1988 September 13; accepted 1989 March 2

ABSTRACT

We present and discuss observational data on the nova remnant GK Persei and its environs at a variety of wavelengths. The spectral range includes six radio wavelengths plus the 21 cm line, *IRAS* data from 100 to 12 μm, and optical images in the continuum and emission lines. The latter includes images at several epochs extending back to the nova outburst in 1901.

The data suggest in a self-consistent manner that the nova exploded into a circumstellar cloud whose mass is estimated to be several solar masses and whose mean diameter is several pc. This cloud is visible both in the *IRAS* data and in the 21 cm data. Radio images of the nonthermal emission associated with the interaction of the nova ejecta with this material show a remarkable similarity to young supernova remnants. This similarity is based on their morphology, distribution of polarization, and in the inferred efficiency of relativistic particle production. The ridge of maximum radio and optical brightness exhibits a remarkable alignment with these circumstellar features, suggesting a related origin.

We examine in detail a suggestion made by Bode *et al.* that the circumstellar cloud surrounding GK Per is the neutral remnant of a planetary nebula which occurred about 10^5 yr ago. The white dwarf in the GK Per binary would then be the stellar remnant of this planetary. In this picture, the explosion of the nova into the planetary nebula accounts for the unique character of GK Per. A model is developed in which the planetary nebula shell is a torus responsible for the *IRAS* emission. Less massive polar outflows along the axis of the torus provide the material necessary to account for the interaction with the nova ejecta and for the brightest parts of the light echo seen in this nova.

Though this interpretation is neither unique nor free of problems, it provides a remarkably consistent framework for the interpretation of all the data.

Subject headings: nebulae: individual (GK Per) — nebulae: planetary — radio sources: extended — radio sources: 21 cm radiation — stars: individual (GK Per) — stars: novae

I. INTRODUCTION

a) *Classical Novae*

The cataclysmic variable (CV) class of objects includes dwarf novae, recurrent novae, and classical novae. These systems are typified by unpredictable outbursts ranging from a few magnitudes for dwarf novae to greater than 18 magnitudes for the most luminous classical novae. The central systems of dwarf novae and classical novae both generally contain a main-sequence dwarf losing matter by Roche lobe overflow, via an accretion disk, onto the surface of a white dwarf primary. Orbital periods are found to be generally in the range 1.5 to 10 hr. Recurrent novae are a small but heterogeneous set of objects, generally having long orbital periods, and in several cases the mass-donating secondary star is thought to be a red giant. The nature of the primary in such systems is ill-defined, as is the cause of the outburst. In classical novae, the outburst is caused by a thermonuclear runaway on the surface of the white dwarf, whereas in dwarf novae the outburst is due to increased accretion through the disk (see Bath 1978 for a review).

At outburst, a classical nova's luminosity will generally be in the range 5×10^{37} to 5×10^{38} ergs s^{-1}. Around 10^{-5} to 10^{-4} $M_\odot$ of material is ejected at velocities of order 1000 km s^{-1}. Statistical arguments have led to the conclusion that the outburst period of classical novae is approximately 10^4–10^5 yr. Such a system may undergo many such outbursts over its lifetime, but the actual lifetime of the classical nova phase is poorly determined (Patterson 1984). In general it is believed that cataclysmic variable systems evolved from longer period binaries which underwent loss of angular momentum, along with large amounts of matter, during a common envelope phase after the primary star became a red giant. See Webbink (1985) for a review of the evolution of CV binaries, and Gallagher and Starrfield (1978) for a review of classical novae in general.

b) *GK Persei*

GK Per (Nova Persei 1901) was the first bright nova of the 20th century and was also the first such object to be subjected to very detailed spectroscopy and photographic photometry (Payne-Gaposchkin 1957). It was discovered on 1901 February 22, and reached a maximum of $V = 0.2$ a few days later. Subsequently, it declined at 0.23 mag per day, making it a very fast nova. It presently resides at minimum with $V = 13.1$ mag typically, with occasional dwarf nova–like outbursts of around 3 mag, which are unusual among classical novae (Sabbadin and Bianchini 1983).

Apart from its dwarf nova–like activity, GK Per is unusual in several other respects. It has by far the longest known orbital period among classical novae (1.904 days, Bianchini, Hamzaoglu, and Sabbadin 1981; 1.997 days, Crampton, Cowley and Fisher 1986). In addition, unlike any other known classical nova it contains an evolved secondary of type K2IV (Crampton, Cowley, and Fisher 1986). There is some controversy about the eccentricity of the orbit. It has been suggested to be highly eccentric ($e = 0.39$, Bianchini, Hamzaoglu, and

[1] Department of Astronomy, University of Toronto.
[2] School of Physics and Astronomy, Lancashire Polytechnic.
[3] Department of Physics, University of Keele.

Sabbadin 1981), or essentially circular (Crampton, Cowley, and Fisher 1986). The primary is a white dwarf whose mass has been given as greater than 0.72 $M_\odot$ by Watson, King, and Osborne (1985), 0.9 $M_\odot$ by Crampton, Cowley, and Fisher (1986), and 1.3 $M_\odot$ by Bianchini, Hamzaoglu, and Sabbadin (1981). The mass of the secondary has been estimated to be in a range of 0.25 $M_\odot$ (Crampton, Cowley, and Fisher 1986) to 0.9 $M_\odot$ (Bianchini, Hamzaoglu, and Sabbadin 1981). The orbital inclination is uncertain, but it must be high. Bianchini and Sabbadin (1983) suggest $i = 66°$, whereas Crampton, Cowley, and Fisher (1986) give $i \leq 73°$.

Bianchini and Sabbadin (1983) suggested that the white dwarf in GK Per must have a strong magnetic field ($B = 5 \times 10^5$ gauss) in order to explain the hard X-ray emission from the system, and the form of the accretion disk emission. Observations using *EXOSAT* in 1983 during an optical outburst (Watson, King, and Osborne 1985) showed the X-ray flux to be modulated with a 351 s period, associated with the rotation period of a magnetized white dwarf.

Following the outburst in 1901, expanding nebulosities were detected photographically about the nova (e.g., Perrine 1902). The apparent superlight expansion of some of these nebulosities was explained by Couderc (1939) as reflection from dust grains lying in a plane intersecting the line of sight to the nova. Only in the case of one other nova (Nova Sgr 1936) have such phenomena been reported (Swope 1940), despite modern searches around recent novae (van den Bergh 1977; Schaefer 1988). The failure of Schaefer (1988) to detect such phenomena in other novae has led him to the suggestion that the grain density in the light-echo region of GK Per is up to 10^4 times that in the general interstellar medium.

The ejecta from the 1901 outburst were first photographed in 1916 by E. E. Barnard and have been followed intermittently ever since. The nebulosity shows an asymmetry unique among novae, and the longevity of the remnant is quite unusual. The total mass ejected has been estimated to be 7×10^{-5} $M_\odot$ (Pottasch 1959), and the ejection velocity is given as 1200 km s^{-2} (McLaughlin 1960). Distance determinations have been performed using expansion parallax, and the most widely accepted value is 470 pc (McLaughlin 1960), although Duerbeck (1981) quotes a value of 525 pc. Here we will take $d = 470$ pc throughout.

By analyzing the evolution of the optical nebulosity over several decades, Oort (1951) concluded that the expanding ejecta were interacting with the ambient medium. The electron temperature in the remnant, determined from optical spectroscopy, is greater than 2.5×10^4 K (Williams 1981), and the spectrum itself looks more like a young supernova remnant than a classical nova shell (Williams 1987). With many of these considerations in mind, Chevalier (1977*b*) concluded that GK Per might be a potential site for relativistic particle acceleration. Indeed, when Reynolds and Chevalier (1984) observed the source with the Very Large Array (VLA) at 1.5 and 4.9 GHz their results showed GK Per to be a nonthermal, polarized radio source with spectral index -0.67 and morphology resembling the optical remnant. A survey of radio emission from novae (Bode, Seaquist, and Evans 1987) determined that such behavior was very unusual. Thus it was that we undertook our multiwavelength study of GK Per in the summer of 1984.

In this paper we present new observations in the radio and optical bands and analyze these along with infrared data from the *IRAS* satellite and archival photographs of GK Per. These data taken together yield considerable new insight into the nature of this unique object and its surrounding environment.

II. OBSERVATIONAL DATA

a) Radio Observations

The radio observations were carried out using four different radio telescopes, namely the VLA,[4] the Westerbork Synthesis Radio Telescope (WSRT[5]), the One Mile Telescope (OMT), and the 5 km Low-Frequency Synthesis Radio Telescope at Cambridge (CLFST), U.K. All observations were carried out during 1984–1986 and include continuum measurements at several frequencies and 21 cm line observations of neutral hydrogen surrounding GK Per. The observations are summarized in Table 1. Only flux densities were measured using the OMT and the 5 km telescope, since these measurements were made at lower frequencies where the resolution was insufficient to resolve the source.

The VLA data were calibrated employing conventional methods, using 3C 48 as a primary flux calibrator. The flux densities adopted for this source at all frequencies were in accordance with the scale of Baars *et al.* (1977). The polarization data were also calibrated using standard procedures adopted at the VLA. The *E*-vector position angle was calibrated using the strongly polarized source 3C 138. The position angle adopted for this source is $-12°$ at both 1.49 and 4.86 GHz. This source was observed four times at 1.49 GHz to check for possible variations in position angle due to ionospheric Faraday rotation. No significant variations were found, and we have assumed that no ionospheric effects were present.

The measurements at 1.49 and 4.86 GHz were made using scaled-array configurations so that the *u-v* plane coverage is the same at both frequencies. These measurements, which produce images with identical resolution, facilitate the measurement of the spectral index and a comparison of the polarization characteristics between these two frequencies.

The WSRT and Cambridge observations were also calibrated using standard procedures at the respective observatories. No polarized emission was detected above the noise in the WSRT 608 MHz (1 σ limit of 1 mJy ba^{-1}). No polarization observations were attempted at 151, 327, 408, or 1407 MHz.

The neutral hydrogen observations were made using the VLA in the D-array configuration. A total of 25 antennas were used, with a correlator configuration of 128 channels and a channel separation of 24 kHz, corresponding to 5 km s^{-1}. Only the inner 32 channels were recorded, centered at 0 km s^{-1} (LSR) for a total velocity coverage of 150 km s^{-1}. In addition to this a continuum channel was obtained, formed from the inner 75% of the total bandwidth (3.125 MHz). The ripple on the IF bandpass was removed using the source 3C 48 as a bandpass calibrator.

b) Far-Infrared Measurements

The *Infrared Astronomical Satellite* (*IRAS*) surveyed 98% of the sky in four wavelength bands with effective wavelengths of 12, 25, 60, and 100 μm (Neugebauer *et al.* 1984). Initial investigation of the region around GK Per was performed using sky

[4] The Very Large Array is operated by the National Radio Astronomy Observatory under contract with the National Science Foundation.

[5] The Westerbork Synthesis Radio Telescope is operated by the Netherlands Foundation for Radio Astronomy (SRZM) under support by the Netherlands Organization for the Advancement of Pure Research (ZWO).

TABLE 1

SUMMARY OF RADIO OBSERVATIONS OF GK PER

Date of Observation	Telescope (Config.)	Frequency (GHz)	Resolution	Type of Observation	Integration Time (hr)	Flux Density (mJy)
1984 Aug 14	VLA (D)	4.860	13".0	Continuum	7.1	8.7 ± 0.5
1985 Aug 08	VLA (C)	1.490	13.0	Continuum	6.2	20.6 ± 1.6
1986 Jan 27	VLA (D)	1.420	40.8	21 cm line	8.4	
1985 Jul 31	WSRT	0.608	35×49	Continuum	12[a]	23 ± 3
1986.6	OMT	0.408	80×116	Continuum	12[b]	33 ± 10
1985 Feb 16	WSRT	0.327	53×77	Continuum	12[a]	$20(+10, -5)$
1986 Feb 08	CLFST	0.151	65×93	Continuum	12	<40

[a] Full synthesis, 16 baseline pairs.
[b] Full synthesis, 40 baseline pairs.

flux maps (Beichman *et al.* 1985). Having discovered an extended source associated with the nova, we decided to use the raw *IRAS* database, for two reasons. First, the full spatial resolution of the instrument at each waveband could be used, rather than the uniformly poor 5′ resolution of the sky flux images. Second, the GK Per region had fortuitously been scanned no fewer than 25 times in both the normal survey mode and in an unrelated deep survey. This meant that by combining the raw data scans we could go around 2–3 times deeper in surface brightness than was the case with the generally distributed data products. Details relating to the *IRAS* data are to be found in Table 2.

IRAS data reduction was performed with computer packages developed on STARLINK by the *IRAS* Post Mission Analysis Facility (IPMAF) at the Rutherford and Appleton Laboratory. Raw data were first selected from the data archive at IPMAF, then examined for striping and obvious hysteresis problems. Selection, destriping and rebinning of the data were performed using the CRDD suite of programs (Stewart 1987). Co-adding was done using I_COMBINE, and finally imaging and flux calculations were achieved using I_CONTOUR (Hirst and Cudlip 1984). Although it was usual to subtract a background from the resulting image as part of the above programs, it was found that this resulted in spurious background levels as the background was fitted by a linear function to all the data on a scan, and not just to the background level in the map area. We therefore produced a map of the region first, then subtracted a background based on measurements in regions of the map where no obvious sources appeared. However, this method, although producing a more reliable background level, did not yield results for total flux that were discrepant from the automatic techniques by much more than the systematic errors associated with the instrument at each waveband.

The noise level in each map was estimated by sampling the background surface brightness in many regions. The errors resulting from map statistics in the integrated fluxes in each band were negligible in comparison to the calibration errors of the instrument. Flux estimates were made by integrating the surface brightness down to the 3 σ contour on the 100 μm map, then using the same area on maps at the other three wavebands. The effects of different sized bins around the source were explored, and it was found that the source flux derived in this way was near the asymptote of flux versus box area for each waveband. In the case of the 12 and 25 μm maps, obvious point sources were excluded from the integration, and a color correction to the fluxes, assuming a 400 K blackbody, was made (Beichman *et al.* 1985) resulting in an increase over the uncorrected flux in band *I* (12 μm) of only 1%, but a decrease of 18% in band II (25 μm). Tabulated values for color corrections at temperatures less than around 30 K are not given in Beichman *et al.*, but judging from those at the lowest temperatures given, the correction to our data at 60 and 100 μm would be of order a few percent, again negligible in comparison to the calibration errors in these bands.

c) *Optical Observations*

Archival photographs of the reflection nebulosity around GK Per seen in 1901 and 1902 taken with the 36 inch (91 cm) Crossley reflector at Lick (e.g., Perrine 1902), the 24 inch (61 cm) reflector at Yerkes (e.g., Ritchey 1901) and the 72 cm Bruce astrograph at Heidelberg (Kopff 1906), together with photographs of the expanding ejecta from 1917 to 1977 from several observatories, have been obtained. The plates, or direct copies thereof, of the reflection nebulosity ("light echo") have been scanned by the PDS 2200-GME of the Astronomical Institute of the University of Münster, and processed using STARLINK software on the Lancashire Polytechnic μVAX. Tables 3 and 4 give details of archival material referred to below. Obviously, not all the material we acquired is presented here, but a selection of the most important and better quality images is shown.

TABLE 2

IRAS DETAILS AND RESULTS

Parameter	Band I	Band II	Band III	Band IV
λ (μm)	12	25	60	100
$\Delta\lambda$ (μm)	6.1	10.4	33.6	30.5
Resolution (arcmin) ..... (inscan × cross scan)	0.7×2	0.7×2	1.2×2	1.5×2
1σ noise (MJy sr^{-1})	0.08	0.1	0.14	0.51
Flux density (Jy)	11.2 ± 0.1[a]	7.8 ± 0.1[a]	40.7 ± 0.3	217 ± 1.5

[a] Color corrected.

TABLE 3

LIGHT ECHO IMAGES

Date	Instrument	Exposure Time	Observer and Institution
1901 Aug 23	Bruce astrograph	4^h 6^m	Wolf, Heidelberg
1901 Sep 20	24 inch reflector	3 20	Ritchey, Yerkes
1901 Nov 12/13	Crossley reflector	10 00	Perrine, Lick
1901 Dec 4	Crossley reflector	5 28	Perrine, Lick
1902 Jan 2/3	Crossley reflector	10 00	Perrine, Lick
1902 Jan 31/Feb 2	Crossley reflector	9 45	Perrine, Lick
1902 Mar 4/6	Crossley reflector	4 15	Perrine, Lick
1902 Aug 13/14	24 inch reflector	6 00	Ritchey, Yerkes

TABLE 4

EJECTA PHOTOGRAPHS

Date	Instrument	Exposure Time	Notes
1917 Nov 15	Mount Wilson 60 inch	?	Ritchey
1937 Oct 6/7	Mount Wilson 60 inch	1^h15^m	
1942 Nov 6/7	Mount Wilson 100 inch	1 30	103aE + RG2
1944 Oct 15/16	Mount Wilson 100 inch	2 00	103aO + UG2
1949 Nov 20/21	Mount Palomar 200 inch	?	
1959 Dec 19	Lick 120 inch	30	103aO + UG2
1972 Sep 8/9	Mount Palomar 200 inch	50	103aE + RG2
1977 Nov 16	Steward Obs. 60 inch	?	Hα + [N II]

Measurement of the print copies of the original plates obtained from Lick Observatory, The Royal Astronomical Society, and the Mount Wilson and Las Campanas Observatories was initially attempted using a measuring engine. However, the errors in position were so large due to the subjective determination of the centers of particular features, that careful measurement with a graduated scale sufficed. The scale of each print was determined by using the accurate stellar positions measured by von Küstner (1921) in the GK Per region. The extent of the reflection nebulosity, or ejecta, in a particular direction was determined with reference to a star measured by von Küstner in that direction to eliminate the effects of any plate curvature.

Optical CCD images of the expanding nebulosity have been obtained through various filters between 1984 August and 1987 July. Details of these observations are to be found in Table 5. The purpose of obtaining these images was to provide insight into the physical conditions of the optically emitting knots.

III. RESULTS

a) IRAS Images of the Regions Surrounding GK Persei

Figure 1 shows images from the *IRAS* data at 12, 25, 60, and 100 μm. The 60 and 100 μm images clearly show the presence of an elongated structure running roughly NW-SE through the position of the nova, and coincident with the H I emission as shown in Figure 3. The total extent of the *IRAS* emission is approximately 40′. The most striking feature of the 60 and 100 μm images is the double-peaked structure of the emission, with the westerly peak in the 100 μm image lying at approximately 5′ from the nova, and the nova itself sitting on a saddle point between these peaks. It is interesting to note that the westerly peak is associated with a point source in the *IRAS* Point Source Catalog (PSC) in bands III and IV at flux levels which are around 20 times less than that derived here. The discrepancy is due to the extended nature of the source which is not assumed in the point source criteria used to determine fluxes for the PSC. Also worth noting is that this "point source" is associated by the SCAR *IRAS* software package (Fairclough and Cooke 1986) with an X-ray source that turns out to be the nova itself.

The 12 and 25 μm images show less dramatic evidence for this bipolar emission, but do nevertheless show some evidence for extended emission in this region. As remarked above however, many point sources appear which are probably unrelated to the extended source around GK Per, particularly in the 12 μm band. These have been excluded when deriving the total flux at these wavelengths in the extended emission. Figure 2 shows the broad-band spectrum of the source derived as described in § II*b* above.

TABLE 5

CCD IMAGES

Date	Instrument	Exposure Time (minutes)	Filter
1984 Aug 19	2.2 m Calar Alto	30	Hα + [N II]
1986 Mar 29	2.5 m Isaac Newton Telescope, La Palma	5	[O III] 5007
1987 Jul 27	2.5 m Isaac Newton Telescope, La Palma	5	*R*
1987 Jul 27	2.5 m Isaac Newton Telescope, La Palma	30	[O II] 3727

b) Neutral Hydrogen Measurements

Maps of the brightness distribution were made for each of the 32 velocity channels, and maps of the line emission alone were obtained for each channel by subtracting the continuum map of bandwidth 2.34 MHz. Uniform weighting in the *u-v* plane was employed and no CLEANing was performed on these maps. No line emission was found in channels 2–14 (10 km $s^{-1} < V_{LSR} < 72$ km s^{-1}), or in channels 25–32 (-86 km $s^{-1} < V_{LSR} < -46$ km s^{-1}). The rms noise level on these maps is approximately 2 mJy, exactly that expected from receiver

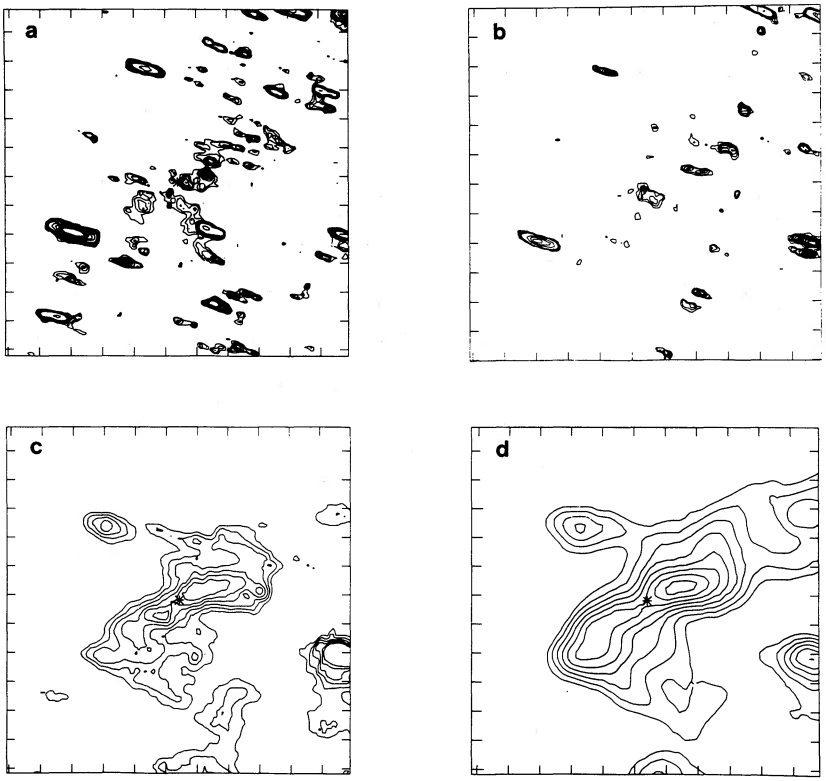

FIG. 1.—Far-infrared emission detected by *IRAS* in the GK Per region. The effective wavelength (μm), base contour level (MJy sr^{-1}, 3 σ above background noise) and contour interval (MJy sr^{-1}) for each image are, respectively, (*a*) 12, 0.18, 0.04; (*b*) 25, 0.23, 0.04; (*c*) 60, 0.27, 0.125; (*d*) 100, 0.5, 0.5. The position of the nova is marked with an asterisk. Axes are marked in intervals of 5′ in declination and 30 s of right ascension.

noise for an integration time of 8 hr. Weak emission was found over the velocity range -41 to 5 km s^{-1}, comparable to that found in the low-resolution survey by Weaver and Williams (1973) containing this region. This emission is very extended, however, and much of it is resolved out by the VLA. The region around GK Per contains emission predominantly at 0 and 5 km s^{-1} as shown in Figure 3. GK Per appears to be embedded in an elongated feature between 10′ and 20′ in length, running from SE to NW. The length and orientation of this emission are similar to those of the *IRAS* emission (see Fig. 1 and § III*a*).

In the field containing GK Per, two field sources, each roughly 15′ away from GK Per, were strong enough to exhibit H I absorption. This absorption is useful for probing the inter-

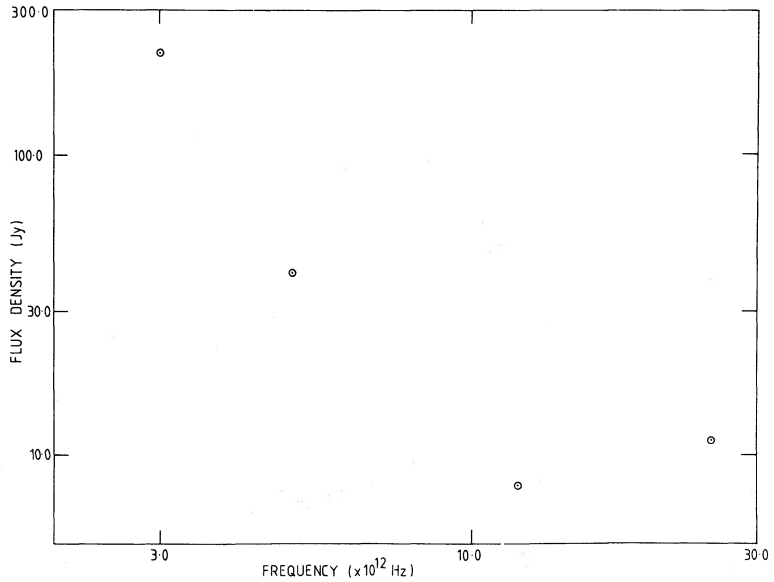

FIG. 2.—Flux density spectrum of the *IRAS* emission (See text for details)

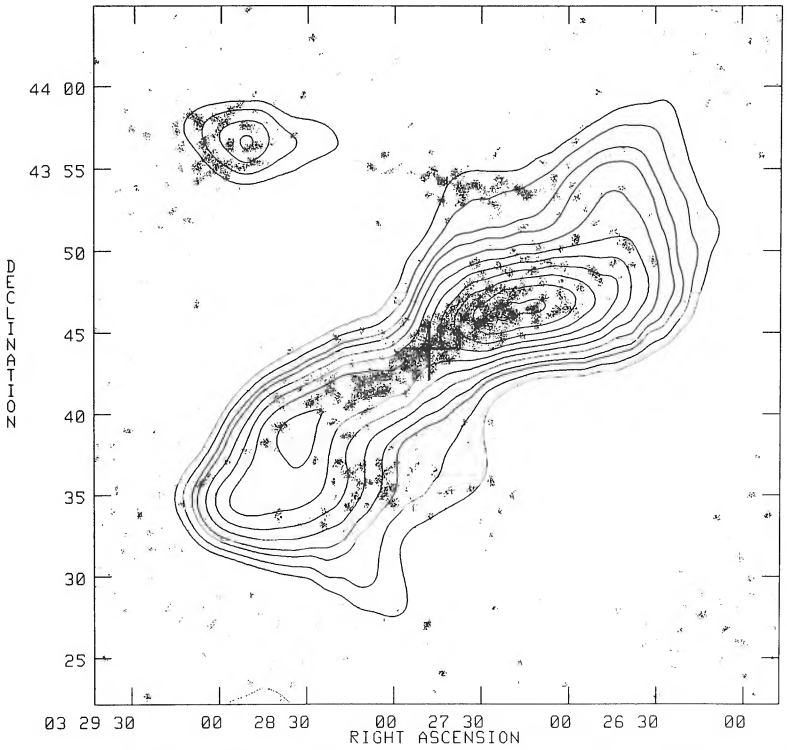

FIG. 3.—Grayscale image of the H I emission in the velocity channels at 0.0 and 5.2 km s^{-1} superposed on a contour image of the 100 μm *IRAS* map of Fig. 1. The mean H I column density within the bounds of the *IRAS* image is 6×10^{19} cm^{-2}. The maximum signal-to-noise in the H I image is 16. The negative *IRAS* contour is at -1.3 MJy sr^{-1}, while the positive contours begin at 1.3 MJy sr^{-1} and increase in steps 0.3 MJy sr^{-1}. The position of the nova is marked by the cross.

stellar gas environment within a projected distance of approximately 2 pc surrounding GK Per. Data on these two sources are given in Table 6.

c) *Radio Continuum Measurements*

The radio measurements of the GK Per remnant are presented both in the form of a spectrum of the integrated radio emission (Fig. 4) and a series of radio images (Figs. 5–7). The integrated flux densities were obtained by integrating the images made from the various telescopes used. All images were deconvolved using the CLEAN algorithm (Högbom 1974), as it is implemented at the various institutions.

Figure 5 shows a radio image at 4.86 GHz superposed on the 1984 Calar Alto Hα + [N II] 6584 CCD image. The radio image has been made with uniform weighting and a Gaussian taper in the *u-v* plane of 12,000 wavelengths at the 30% level. This taper was chosen as an optimum between resolution and sensitivity for comparison with the optical data. The rms noise level on the 4.86 GHz is 25 μJy, approximately consistent with that expected due to noise in the receivers.

The position of the nova remnant in Figures 5–7 differs from the 5 GHz image of Reynolds and Chevalier (1984) by 15″. This discrepancy could not be produced by the observed expansion velocities. The symmetrical placement of the nova remnant with the nova itself, and the alignment of our radio and optical images (Fig. 5) suggests that our position is the correct one, and that the Reynolds and Chevalier image is in error.

Images of the VLA data were also made at 1.49 and 4.86 GHz using natural weighting in the *u-v* plane. This weighting gives the highest signal-to-noise ratio for unresolved sources but produces lower resolution compared to the image in Figure 5. These images were judged to be optimum for conveying the distribution of polarization and spectral index. Figure 7 shows these radio images at the two frequencies with polarization *E*-vectors superposed, and corresponding maps of the distribution of the percentage linear polarization. The maps of polarized intensity used to produce Figure 7 were corrected for polarization noise bias before calculating the percentage polarization. This was done using an AIPS algorithm, which employs a method derived from Killean, Bicknell, and Ekers

TABLE 6

FIELD SOURCES DETECTED IN H I ABSORPTION

Source	R.A.(1950)	Decl.(1950)	1.49 GHz Flux (mJy)	Optical Depth	V_{LSR} (km s^{-1})	FWHM (km s^{-1})
A	$03^h27^m08^s$	43°29′50″	81.1	0.23	−4.4	12.7
B	03 28 17	44 03 00	85.3	0.34	−3.5	10.0

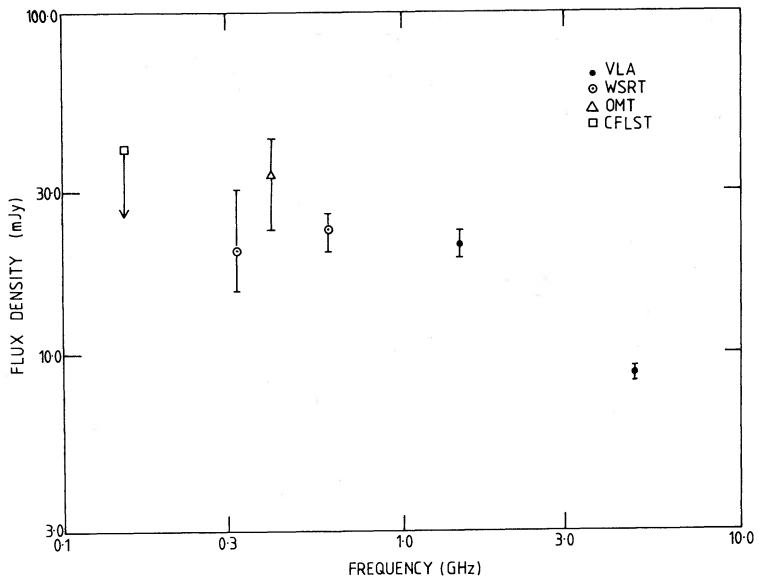

FIG. 4.—The radio flux spectrum of GK Per (See text for details)

(1986). This algorithm blanks polarization signals that are less than twice the rms noise in either Stokes parameter. The signals in the percentage polarization images were also blanked when the total intensity fell below the 4 σ level.

Figure 8 shows the distribution of the spectral index α, defined by $S_\nu \propto \nu^\alpha$ and determined between 1.49 and 4.86 GHz, across the image. This distribution was found to be slightly affected by a plateau of background emission surrounding GK Per at 1.49 GHz. This plateau has a brightness of about 70 μJy ba^{-1}, close to the noise level. This plateau is probably related to confusion in the field surrounding GK Per. Spectral index maps were made before and after subtracting this plateau. A comparison of the two maps showed a maximum difference of 0.1 in the spectral index in the weaker regions toward the

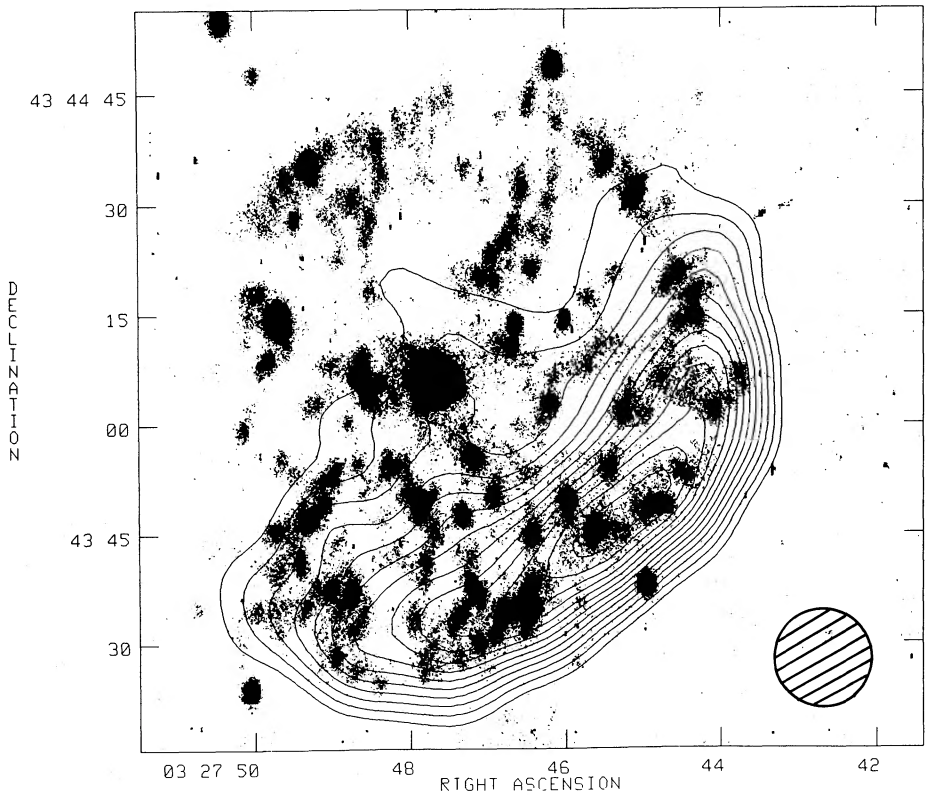

FIG. 5.—Radio contour image at 4.86 GHz superposed on a grayscale [N II] image. The radio map was made with a Gaussian u-v taper of 12,000 wavelengths at the 30% level, for a beamwidth of 13″ (shown at lower right). Contour intervals increase from 6 to 32 times the rms noise (25 μJy ba^{-1}) in steps of 2.

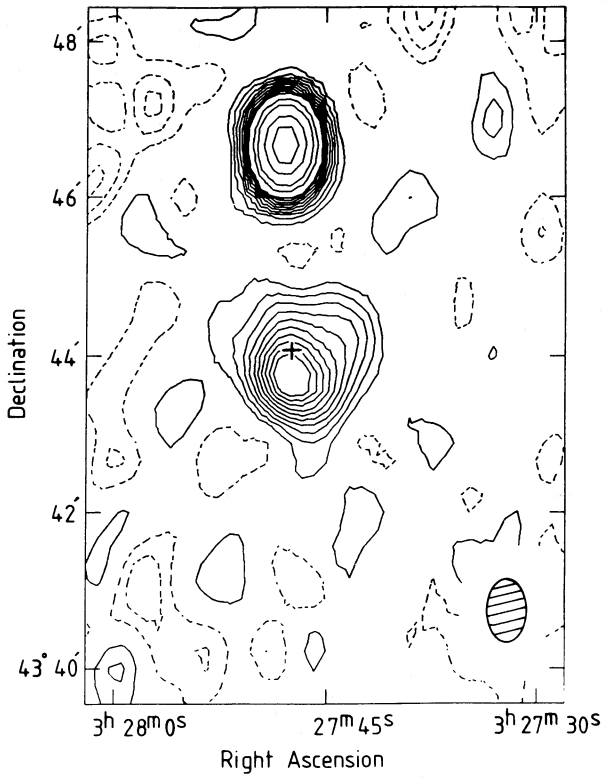

FIG. 6.—Radio image of the GK Per region at 608 MHz made with the WSRT. Contour levels are at -3 to 10 mJy ba^{-1} in steps of 1 mJy ba^{-1}, with negative contours shown as dashed lines, and the zero contour omitted. Above 10 mJy ba^{-1} the contour levels are 15, 20, 30, 40 mJy ba^{-1}. The cross marks the position of the stellar system. The oval shows the FWHP beam. The point source due north of GK Per has a flux density of 52 ± 1 mJy at 608 MHz.

north. The image in Figure 8 was made after the removal of this plateau. The random error in the spectral index image due to noise varies from 0.03 where the brightness is most intense to 0.3 in the contour at the edge of the spectral index image.

d) Optical Images

Figures 9 and 10 (Plates 16–19) show a selection of the best images of the reflection nebulosity and the expanding ejecta. Figure 11 (Plate 20) shows the optical CCD images. It has proved impossible to determine what emulsions and filters were used for all the archival photographs, but it is safe to assume that the earliest photographs were unfiltered, on blue-sensitive emulsions. The Hα filtered images are in fact predominantly mapping the [N II] 6584 line which falls within this broad filter. This line is at least 20 times as strong as Hα in the remnant (Duerbeck 1987*a*).

The 1986 image obtained with the Isaac Newton Telescope shows the distribution of [O III] 5007 emission, while the latter two, taken with the same instrument in 1987, show the emission through the *R* filter and the [O II] 3727 doublet, respectively. These last two images have had backgrounds removed using a polynomial fitting routine developed for *IRAS* data (Hughes, Appleton, and Schombert 1988), and have then been smoothed with a Gaussian with $\sigma = 2$ pixels to enhance diffuse emission on the [O II] image. The same procedure was followed for both images to allow direct comparison.

The distribution of the reflection nebulosity to the south of the nova, the appearance of a "chevron-shaped" feature to the southeast (indicated by an arrow on Fig. 9 [Pls. 16–17]), the movement of the nebulosity between epochs, and a "static" feature in the southwest can clearly be seen on Figure 9. The earliest photograph of the ejecta (taken in 1917) and all subsequent images (see Figs. 10 and 11) show that the central remnant is highly asymmetric, with the bulk of the emission arising in the SW quadrant in all but the [O III] CCD frame. The later images also suggest a box-shaped morphology, with evident flattening in the SW and NE. The striking contrast between the distribution of [O III] and [N II] ([O II]) emission is clear from these frames.

IV. DISCUSSION

In this section we present a comprehensive interpretation of the data on GK Per. We begin with a discussion of the environment surrounding the nova on a spatial scale of up to several parsecs, and then discuss the interaction of the nova ejecta with this environment. Finally, we present the impact of our conclusions on our understanding of the central system.

a) The Circumstellar Environment

A preliminary discussion of the ambient medium into which the ejecta are moving is given by Bode *et al.* (1987). These authors argued that the bipolar morphology of the *IRAS* emission surrounding GK Per suggeststs that it is an ancient planetary nebula (PN), a point that we will discuss in more detail below. Here we address the properties of the circumstellar medium in general terms. We discuss, in turn, the IR emission, the 21 cm emission, and the interpretation of the light echos of the nova detected immediately after the outburst.

i) *Far-Infrared Emission*

Measurement of the ratio of fluxes at 60 and 100 μm across the *IRAS* nebulosity yields $f60/f100 = 0.175 \pm 0.015$, a value similar to that found for the infrared cirrus. The latter is associated with emission from grains with radii 0.01–0.1 μm in the interstellar medium, heated by the ambient stellar radiation field (Low *et al.* 1984). Further evidence for the similarity of the emission around GK Per to that from the cirrus comes from the detection of the source at 12 and 25 μm where a linear extrapolation of the longer wavelength fluxes would suggest no detection would be made. This short-wavelength excess is attributed to the presence of a population of very small grains with radii 3–10 Å (Weiland *et al.* 1986) possibly in the form of polycyclic aromatic hydrocarbons (PAHs; Habing 1988). It is also intriguing to note that a strong correlation has been found to exist between the distribution of CO (Weiland *et al.* 1986), H I (Habing 1988), and the cirrus. Although the H I emission correlates well with the *IRAS* emission here (Fig. 3), ^{12}CO($1 \rightarrow 0$) emission mapped by Hessman (1987) correlates better with the reflection nebulosities. We have also considered the possibility that the emission in *IRAS* bands III and IV might be due to O III and N III fine-structure lines. The results of Zelick (1977) suggest that if line emission alone were responsible for the *IRAS* emission at 60 and 100 μm, then $f60/f100 \geq 6$, far greater than is actually observed (see above). We can therefore rule out fine-structure lines as the primary cause of emission in these bands.

Bode *et al.* (1987) used the results of Draine (1985) for graphite and silicate grains to derive an effective temperature $T = 22 \pm 1$ K for the dust in the *IRAS* nebulosity. Knowing the total flux at 100 μm, this enabled a dust mass of 0.058 $M_\odot$ to be determined for graphite grains, and 0.078 $M_\odot$ if the grains are purely silicates.

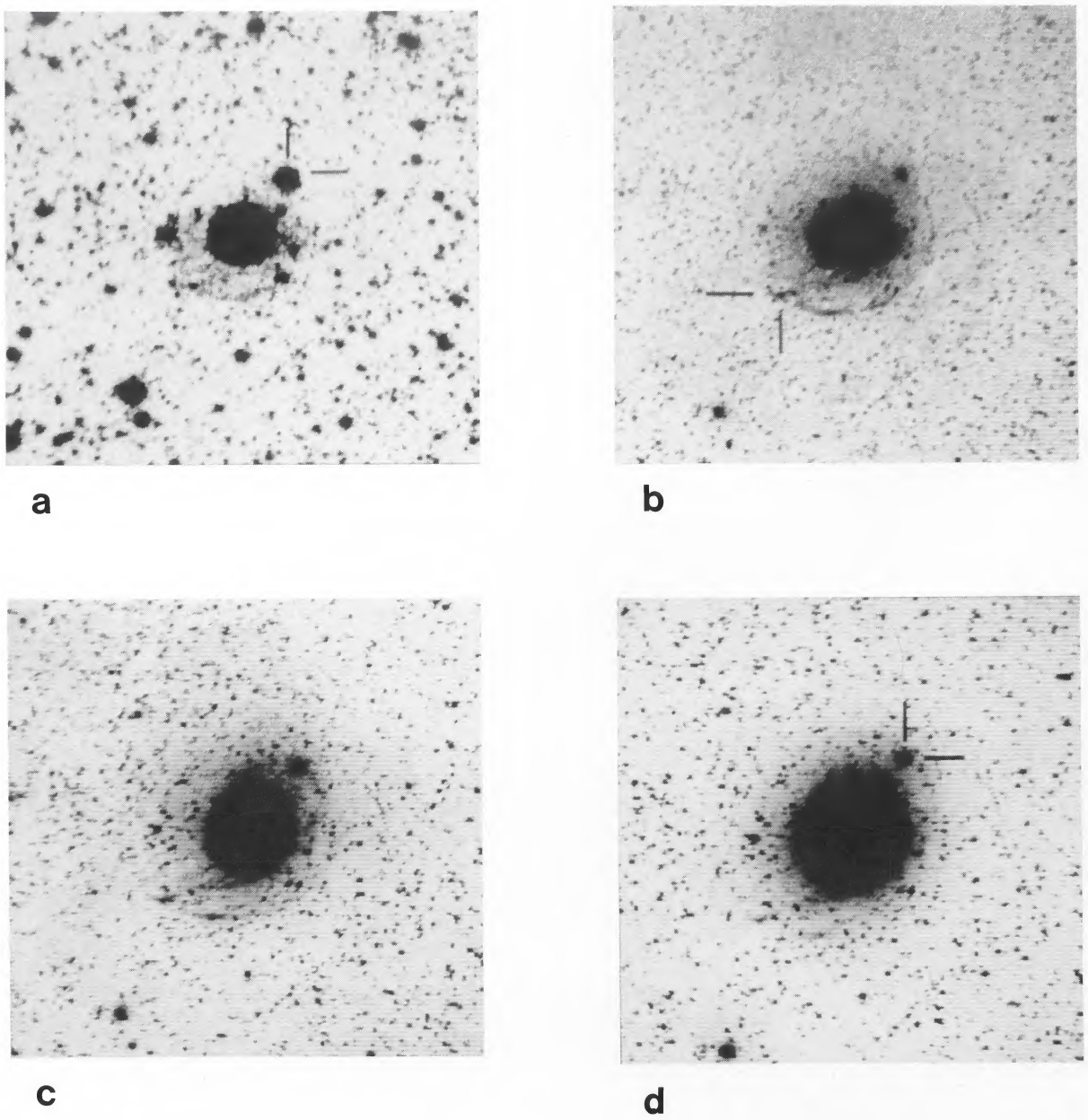

FIG. 9*a–d*

FIG. 9.—Photographs of the light echos around GK Per taken (*a*) 1901 Aug. 23, (*b*) 1901 Sep. 20, (*c*) 1901 Nov. 12, (*d*) 1901 Dec. 4, (*e*) 1902 Jan. 2, (*f*) 1902 Jan. 31, (*g*) 1902 Mar. 4, (*h*) 1902 Aug. 13 (see Table 3 for further details). The "chevron feature" is marked in frames B and F. The "static feature" is at the east end of the horizontal bar in frame E. All images are the result of scanning with the University of Münster PDS, and image processing using STARLINK software. The reference star marked in all frames is approximately 5′ from the nova. All plates have north at the top, west to the right.

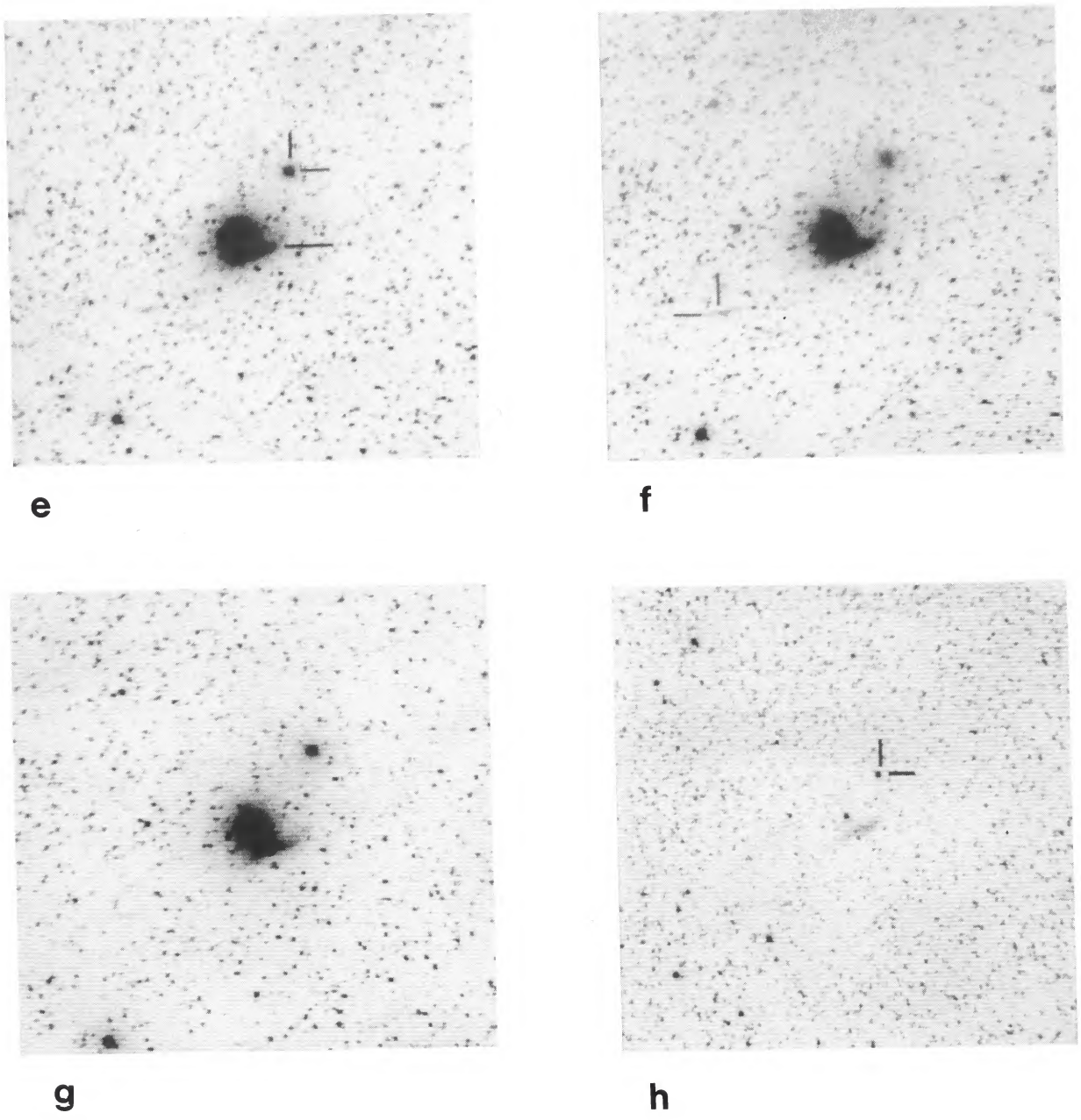

FIG. 9*e–h*

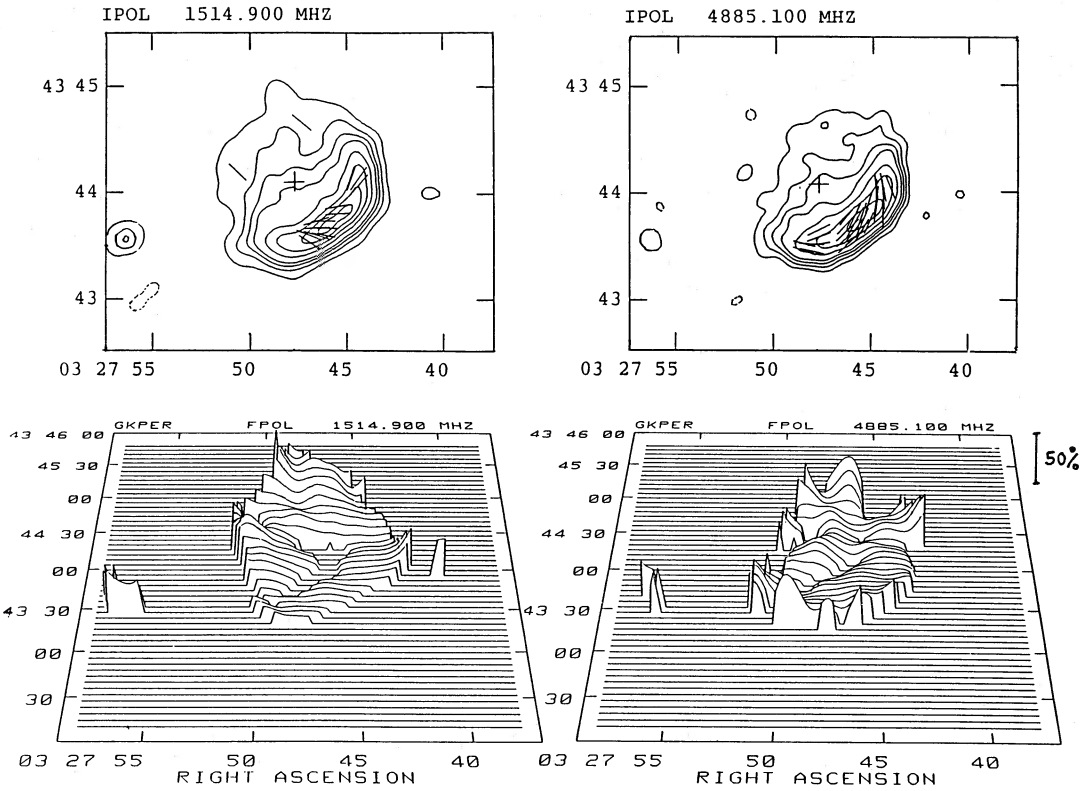

FIG. 7.—Naturally weighted maps at 1.49 and 4.86 GHz showing the distribution of polarized emission. The upper two maps show the *E*-vectors superposed on the total intensity. At 1.49 GHz contours are $-1, 2, 3, 4, 6, 8, 10, 12$ times 0.15 mJy ba^{-1} and the polarization vectors are 10 μJy ba^{-1} arcsec^{-1}. At 4.86 GHz contours are $-1, 1, 2, 3, 4, 6, 8, 10$ times 0.07 mJy ba^{-1} and the polarization vectors are 6.7 μJy ba^{-1} arcsec^{-1}. The lower two maps show the distribution of percentage polarization with the scale as indicated. The cross marks the position of the nova.

Having determined the mass of dust that could give rise to the observed *IRAS* emission, we now turn our attention to the morphology of the cloud. Measurements of the color temperature across the nebulosity show no evidence for a variation larger than the error of 1 K. Essentially, the cloud is isothermal and is therefore not being significantly heated centrally by the nova remnant. This strengthens the assumption that the dust is being heated by the ambient interstellar radiation field, in the same way as the infrared cirrus. We may note here that if the relationship between surface brightness and A_v for the cirrus (de Vries and le Poole 1985) also pertains to this nebulosity, then the peak visual optical depth in the cloud should be around 0.6. This compares to the interstellar extinction at the distance of the nova of 0.9 mag $\pm$ 0.2 mag estimated from extinction mapping in the optical, and an upper limit to the local extinction in the halo and *IRAS* nebulosity of $A_v < 0.4$ mag (Roberts *et al.* 1988).

That the emission is bipolar, with the nova sitting on a saddle point between two peaks of emission, not only suggests that the nova is associated with the cloud, but that the true shape of the cloud is a toroid surrounding the nova. Bode *et al.* (1987) first considered the possibility that the nova lies fortuitously close to a small interstellar cloud. The central cavity in the toroid could then be formed by (*a*) sputtering, or (*b*) sweeping up in the shock wave generated as the ejecta from an outburst encounters the cloud, or by direct evaporation of grains by the radiation flux from the outbursting nova. Simple consideration of the dynamics of a shock moving into a uniform medium, with the density derived from the H I observations, showed that the time scale for the shock to become well-cooled, and hence decrease rapidly in velocity, was less than either the sweeping-up time or sputtering time of the grains, and occurred at a radius which was a factor of 10 less than the observed cavity radius. It was also shown that the evaporation radius at nova outburst is a factor of 10^4 smaller than that of the cavity. The main conclusion to be drawn from these findings is that the toroid is most likely the result of an ejection event associated with the central binary, but the mass of the nebulosity, being 10^4 times that of the ejecta at outburst, cannot be associated with a normal nova event. We do, however, know that the central binary contains a white dwarf star and a late-type subgiant which may be very evolved for the lower limits to its implied mass (i.e., 0.25 $M_\odot$; Crampton, Cowley, and Fisher 1986). The interpretation of the *IRAS* nebulosity in terms of a PN ejected from the system, possibly during a common envelope phase of binary evolution, is discussed more fully in § IV*e* below.

ii) *The* H I *Feature*

The linear H I emission feature shown in Figure 3 is apparently associated with GK Per. This interpretation is suggested by the orientation of this feature which is elongated northwest to southeast, essentially parallel to the synchrotron-emitting ridge in GK Per, and the placement of GK Per relative to the H I emission region. This feature is most prominent at $V_{LSR} = 0$ and 5 km s^{-1}. If the H I cloud were interstellar, emission in this velocity range would support the conclusion that this hydrogen is located within a few hundred parsecs of the Sun, since more distant hydrogen in this direction would be at negative velocity. However, if the H I cloud is part of an expanding

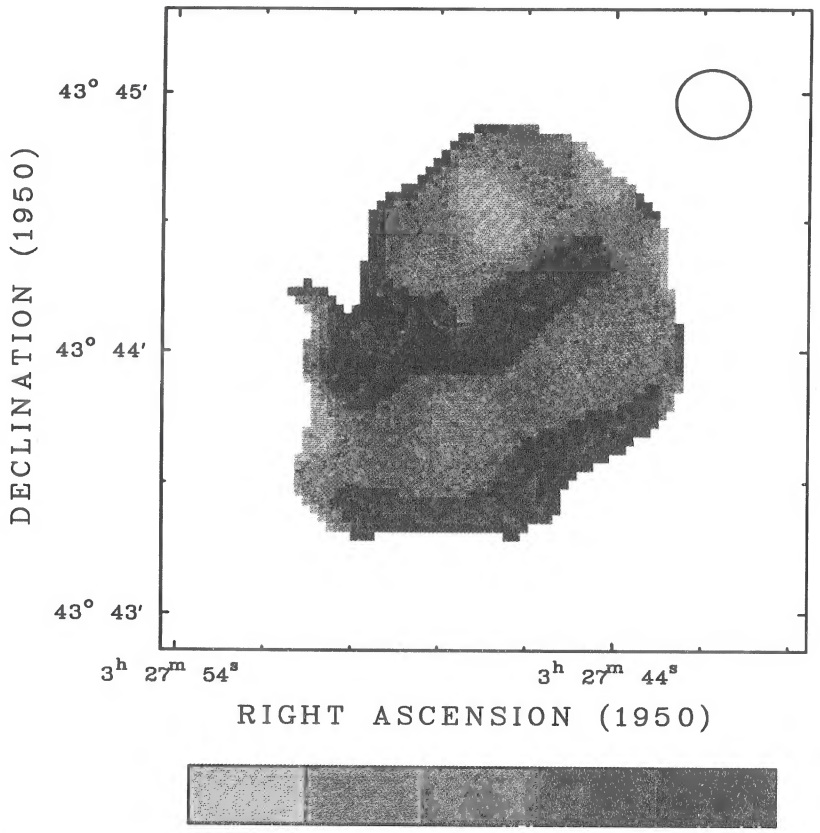

FIG. 8.—The distribution of spectral index between 1.49 GHz and 4.86 GHz. Natural weighting was used, and a plateau region was removed at 1.49 GHz as discussed in the text. The transition values of the spectral index steepens toward darker shades from −0.55 to −0.95 in steps of 0.1. The beam size and its orientation are indicated in the upper right corner. The cross marks the position of the nova.

circumstellar shell, then the velocity cannot be used so straightforwardly to estimate its distance.

The column density of this H I feature has a mean value of about 0.6×10^{20} cm^{-2} within a region of dimensions 0.6 × 0.9 pc, if it is at the distance of GK Per. If the depth is also 0.6–0.9 pc, then the mean density is 20–30 cm^{-3} and the total mass is approximately 0.6 $M_{\odot}$. However, this is probably a lower limit since incomplete short spacing data inherent in maps produced by aperture synthesis means that the more extended emission present may not be represented in our maps. Combining the above H I mass with the mass of dust derived earlier leads to a corresponding upper limit on the dust-to-gas ratio in the nebulosity of 0.09. Since this estimate is an order of magnitude higher than that found in the general interstellar medium (Savage and Mathis 1979) it suggests that as much as 90% of the mass of the H I may be resolved out in these interferometric observations. It should also be noted, however, that a higher dust-to-gas ratio may be plausible if this cloud is not purely interstellar in origin. We return to this point later.

The H I absorption seen against the two nearby discrete sources in our maps (see Table 6) contains information about interstellar (and possibly circumstellar) hydrogen in the direction of GK Per. Both sources are probably extragalactic, and the absorption therefore sheds light on the spin temperature and column density of H I gas along a line of sight passing within about 2 pc projected distance of GK Per. Unfortunately neither of these sources coincides with the main bipolar IR feature, although the northeast source coincides roughly with a weaker IR feature lying on an axis perpendicular to the bipolar axis. The emission profile seen in the Berkeley low latitude survey (Weaver and Williams 1973) shows two components, one broad feature at negative velocity, and one narrow feature centered near 0 km s^{-1}. The shape of the latter component nearly matches that of the two absorption profiles. The former feature is probably associated with distant hydrogen, and the latter feature is undoubtedly gas in the local spiral arm. If we identify the latter feature with hydrogen producing the absorption profile, then the combined absorption and emission may be used to estimate the spin temperature of the gas, presumably in the local arm. Using both absorption profiles, and 20 K for the antenna temperature of the emission component (estimated from the profile in Weaver and Williams 1973), we obtain 70 K $< T_s <$ 100 K for the spin temperature. The corresponding column density ($N_{\rm H\,I}$) is 5.4×10^{20} cm^{-2}. Since the path length to the edge of the H I layer (assuming a semi-thickness of 100 pc) in this direction ($b = -10°$) is about 570 pc, then the mean density of H I along this path is 0.3 cm^{-3}, not significantly different from the density of the local interstellar hydrogen. The column density of the absorbing hydrogen gas gives a lower limit for $E(B-V)$ of 0.12 mag (Heiles 1976). More direct determinations in the UV (Wu *et al.* 1988) and optical (Roberts *et al.* 1988) give $E(B-V) \simeq 0.3$ mag.

iii) *The Light Echo*

The optical light echo observed in 1901 and 1902 poses several important questions. As mentioned in § I, GK Per is one of only two novae where identification of a light echo has been made, and the one associated with Nova Sgr 1936 (Swope 1940) is certainly less well observed, and rather fainter. This phenomenon adds weight to the suggestion that GK Per is immersed in a dense ambient medium, possibly in the form of an interstellar cloud. The fact that the brightest portions of the light echo lie in the same general direction from GK Per as the radio remnant (although the latter is much closer in) may suggest at first sight that the ejecta are interacting with material associated with the light echos. However, Couderc's model of the light echos involved a slab of material whose closest approach to the nova is 14 pc, for his derived nova distance of 625 pc. Reynolds and Chevalier (1984) pointed out that the material in Couderc's model was thus too distant from the nova to be responsible for the interaction that is observed at optical and radio wavelengths. A further problem for the simple Couderc model is to explain the chevron-shaped features that are evident on the 1901 and 1902 photographs, suggesting that a more complex geometry than a simple plane slab may be responsible.

A correlation has been found between infrared cirrus and reflection nebulosities (de Vries and Le Poole 1985). When the *IRAS* data were consulted therefore, it was expected that infrared emission would be found coincident with the position of the light echo. However, the light echo and the *IRAS* nebulosity are largely anticoincident, at least as far as the outer arc is concerned. Part of the reason for the apparent lack of expanding light echos toward the *IRAS* peaks may be that the scattering angles would be large, and the surface brightness would be suppressed if the particles are forward scattering. In addition, the echo would be delayed because the scattering would not be occurring predominantly in regions in front of the nova. The inner portion of the reflection nebulosity does in fact coincide to some extent with the *IRAS* nebula and appears static throughout the epochs over which the photographic record exists. This suggests that the inner part of the reflection nebulosity is of limited extent, at least in the direction in which the expanding arcs are seen. In addition, the prominent chevron to the SE appears to track along the edge of the SE ridge of *IRAS* emission. It should be noted in general, however, that some of the details drawn by Ritchey (1901) are not easily apparent on the high-quality contact negatives of the original plates that we have acquired, and thus should perhaps be treated with some caution. The overall aim here must be to find some model which forms a more consistent picture of the light echos, bearing in mind all the other phenomena of this system to which they seem to be related.

One of the best images of the reflection nebulosity is the 1901 September 20 photograph (Fig. 9). The bright arc to the SW is a very good approximation to the arc of a circle, centered approximately 2'.1 NE of the nova. A line joining the center of this imaginary circle with the nova intersects the near-point of the arc to the nova, and lies at position angle 215° ± 5° (counterclockwise). This is remarkably similar to the position angle of the line joining the nova to the center of the radio ridge, where interaction of the ejecta with the ambient medium is thought to be occurring (see Fig. 5). We now discuss in more detail what the simple geometry can tell us about the distribution of material responsible for the main arc of the light echo.

Figure 12 shows the geometry of the situation. If an observer at O sees an outburst of the nova at N, at time $t = 0$, then he will see scattering of light from the initial outburst from point P, at a time t' later, given by

$$t' = \left(\frac{r_1 + r_2 - d}{c}\right), \tag{1}$$

where distance $\overline{\mathrm{NP}} = r_1$, $\overline{\mathrm{PO}} = r_2$, and d is the distance of the nova from the observer. The scattering surface thus forms an ellipsoid of revolution with the nova and the observer at the foci.

If P lies on a plane of material, inclined at angle γ to the line of sight, then the distance d_1 ($\overline{\mathrm{OR}}$ in Fig. 12, where the point R is defined by a perpendicular from the scattering at P to the line-of-sight $\overline{\mathrm{ON}}$) is given by

$$d_1 = \frac{\cos\alpha_1(c^2t'^2 + 2dct')}{(2ct' + 2d - 2d\cos\alpha_1)}, \tag{2}$$

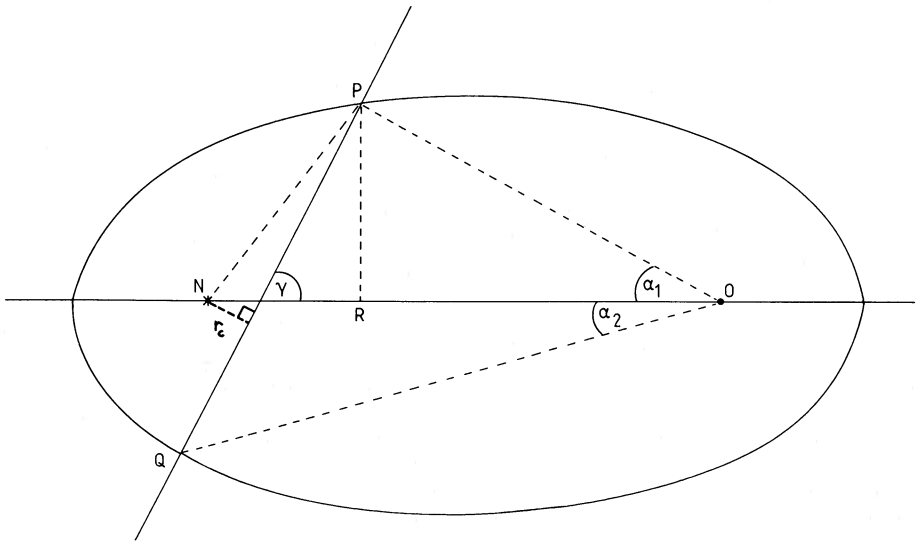

FIG. 12.—Geometry of the light echo (see text for details)

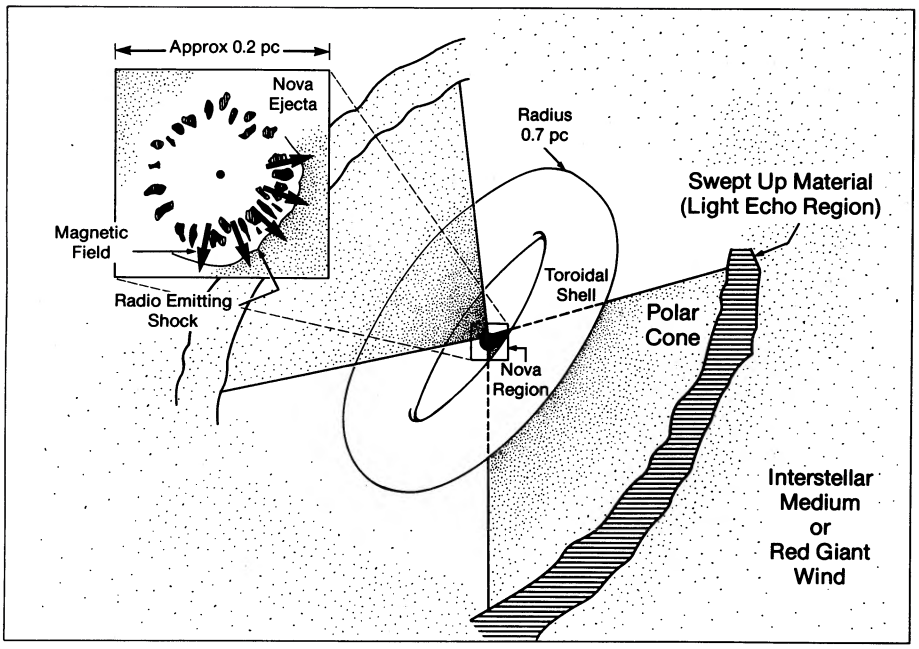

FIG. 13.—Schematic showing the relationship among the various features presumed to be responsible for the observed phenomena in GK Per

where α_1 is the angle of displacement of P from N as seen by O. For $\gamma < 90°$, $\alpha_2 < \alpha_1$, and it can be shown that to a good approximation the observer sees a circle of scattered light whose center is thus displaced from the nova by an amount $\beta = (\alpha_1 - \alpha_2)/2$, where α_2 is angle NOQ.

On 1901 September 20 ($t' = 210$ days), the near point of the southern arc (equivalent to α_2) was approximately 5'.5 from GK Per, and $\beta = 2'.1$. Knowing α_2 and β, and therefore α_1, the inclination of the plane to the line of sight, γ, can be found from

$$\gamma = \tan^{-1}\left(\frac{d_2 \tan \alpha_2 + d_1 \tan \alpha_1}{d_2 - d_1}\right), \quad (3)$$

where d_2 is determined from equation (2), substituting α_2 for α_1. Similarly, the distance of closest approach to the nova of the plane, r_c, can be found from

$$r_c = d_2 \tan \alpha_2 \cos \gamma + (d - d_2) \sin \gamma . \quad (4)$$

Taking $d = 470$ pc, d_1 and d_2 were computed from equation (2), and γ and r_c from equations (3) and (4), respectively. We find that if the scattering material is in the form of a plane (as suggested by the nature of the arc), then $\gamma = 32°$, and $r_c = 1.4$ pc (errors in these quantities are estimated to be of the order of 20%). Thus, r_c is comparable to the radius of the toroid suggested to account for the *IRAS* emission (~ 0.7 pc). In addition, this result suggests that there is matter nearer to the nova than that found by Couderc. The main reason for this is that Couderc used measurements of a much fainter outer arc, sketched by Ritchey, and just visible on the images for 1901 September, and 1902 January, February, March, further from the nova than the much more prominent arc that we have measured.

For the 1901 August 23 Heidelberg plate (day 179), absolute calibration in surface brightness has now been achieved (Roberts 1989). A value of 3.4×10^{-21} W cm^{-2} μm^{-1} arcsec^{-2} (23.2 mag arcsec^{-2}) at ***B*** for the brighter portions of the echo has been determined. Roberts (1988) has constructed detailed time-dependent models of the brightness of scattered light produced by a slab of grains inclined to the line of sight. The model parameters for the slab are the grain number density n_g and grain radius a. The nova outburst is characterized by a light curve of the form $L = 0$ ($t \leq 0$), $L = L_0 e^{(-t/\tau)}$ ($t > 0$), where L is the photographic luminosity, and L_0 and τ are fixed by the light curve of GK Per to be 5.52×10^{32} W μm^{-1} and 4.37 days, respectively. Grain-phase functions were calculated using the Henyey-Greenstein approximation, with asymmetry parameter g taken from Draine and Lee (1984), as are scattering efficiencies Q_{sca}. Using silicate grains, with $a = 0.1$ μm, Draine and Lee give $g = 0.55$, and $Q_{sca} = 1.47$ at ***B***.

The width of the echo, its extent, the limit of $A_v \leq 0.4$ mag in the light echo material (see § IV*a*(i)), and the value of r_c we have derived lead to a slab thickness of around 0.15 pc and a grain density of 2.1×10^{-11} cm^{-3} in the slab. This is around 40 times greater than that found in the general interstellar medium (Allen 1976) and around 100 times less than that found by Schaefer (1988) from a less detailed model, and very roughly estimated echo surface brightness from the 1901 September 20 photograph. It is of interest to note that if we neglect the constraint on the value of r_c arising purely from the geometry, and consider only the estimated surface brightness, any slab could not be situated much farther from the nova without becoming optically thick. Even then, this would only help to increase the allowed distance to a limited extent. Certainly, the scattering material cannot be as far as 14 pc from the nova as suggested by Couderc, even if the estimated surface brightness is greatly in error. We note here that some of the CCD frames listed in Table 5 were obtained several months after a "mini-outburst" of GK Per that occurred in 1986 November (Schweizer, Mattei, and Hurst 1986). The time interval between the mini-outburst and the CCD observations is similar to that between the 1901 nova outburst and the detection of the expanding nebulosity (Perrine 1902); however, no light echo was visible in the CCD data.

Our main conclusions from consideration of the light echos are that the densest part of the scattering material responsible

for the most prominent arc in the SW quadrant lies at a distance from the nova that is remarkably similar to the radius of the *IRAS* nebulosity, if this is also at the distance of the nova. As the idealized slab is found to be of such limited thickness, and the material almost certainly extends back to the interaction region at around one-tenth this distance, it is likely that the density of material increases away from the nova, to peak at this leading edge, then falls away very sharply. The concentration of the echo to the SW suggests the slab is not continuous. The brightest portion of the echo (i.e., the chevron) arises from the edge of the *IRAS* nebulosity, and the grain densities estimated for these two phenomena may well be similar, suggesting a causal link. The association with other fainter structure to the NE has yet to be explored. It is possible, for example, that the IR emission in the NE, but not so clearly in the SW, signifies the presence of dust concentrated along the axis of the toroid. Some of this dust is sufficiently dense to produce the visual light echo, and sufficiently transparent to permit observation of this echo. We return to this point in § IV*e*.

b) Physical Conditions in the Nebular Remnant

i) *Radio Data*

The ridge of maximum radio brightness coincides with a flattened portion of the optical shell in the southwest, and therefore it acts as a tracer of the interaction between the nova ejecta and the ambient gas. Figures 4 and 8 show clearly that the spectrum of the radio emission is nonthermal and that it is polarized. The tangential alignment of the polarization ***E***-vectors at 4.9 GHz is similar to that in young supernova remnants (Milne 1987). We conclude that the emission mechanism is predominantly synchrotron radiation. Above 1 GHz the spectral index is approximately -0.7, and the radio spectrum clearly turns over at lower frequencies with a bend in the spectrum occurring at about 1 GHz. These considerations together with the shell-like morphology of the radio emission lead to the conclusion, in agreement with Reynolds and Chevalier (1984), that in many respects this object behaves like a supernova remnant (SNR) in miniature. The relativistic electrons and magnetic field geometry in the ridge to the southwest are produced by an interaction between the expanding ejecta and ambient gas, either circumstellar or interstellar.

It is worth drawing attention to some differences between GK Per and young supernova remnants as well, however. The maximum degree of linear polarization is 20% at 4.9 GHz, somewhat greater than the maximum of 15% in SNRs (Reynolds 1988). Unlike GK Per no SNRs are known to have a low-frequency turnover as high as 1 GHz. Thus GK Per is somewhat unique, even as a scaled-down SNR.

ii) *The Magnetic Field Strength and Structure*

We have estimated the magnetic field strength in the shell using the usual equipartition arguments (e.g., Pacholczyk 1970). The brightness profile measured along an axis perpendicular to the ridge was fitted to a model consisting of two components, each with its own uniform intensity and angular width. One of these components represents the ridge and the other the low-level plateau of emission interior to the ridge. The brightness levels and widths of these components were adjusted, convolved with a Gaussian beam of 13″ (the FWHM synthesized beamwidth), and fitted to the observed brightness profile. A good fit was obtained with brightness levels in the ridge and plateau of 4.24 and 1.06 μJy arcsec^{-2}, respectively. The corresponding angular widths are 15″ and 60″. Therefore, the ridge is barely resolved by the 13″ beam. The magnetic field strength was computed from the model brightness levels using equation (3) of Miley (1980). The results for the ridge and plateau are respectively 75 and 47 μG. These figures are in good agreement with the equipartition field computed by Reynolds and Chevalier (1984) using an entirely different geometrical model. The corresponding total magnetic energy is 10^{43} ergs, with comparable energy in relativistic particles. Since the total kinetic energy of the ejecta is about 10^{45} ergs, the efficiency of conversion of mechanical energy into magnetic fields and high-energy particles in the shock is about 1%, similar to but perhaps somewhat greater than that for young supernova remnants.

Inspection of Figure 7 shows that the ***E***-vectors at 4.86 GHz are highly ordered indicating a prevailing magnetic field direction which is radial. Note also that there is significant Faraday rotation between 1.49 and 4.86 GHz, amounting to about $-40°$. The (minimum) Faraday rotation required to produce this effect is approximately -20 rad m^{-2}. The average galactic Faraday rotation in this direction ($l = 150°$, $b = -10°$) estimated from maps published by Sofue and Fujimoto (1983) is -40 rad m^{-2}. These maps are based on observations of extragalactic sources, and refer to path lengths through the entire Galaxy. It would be expected therefore that the Faraday rotation along the path to GK Per would be less than this, as observed. Thus all of the observed rotation may be accounted for by the interstellar medium between the Sun and GK Per. There is, however, depolarization at 1.49 GHz relative to 4.86 GHz, as may be seen from Figure 7. A comparison of the percentage polarization maps shows that the percentage at the two frequencies is comparable everywhere except along the bright ridge, particularly where the [N II] and [O II] brightness is large. This depolarization must be due to Faraday effects, which we will argue in the following subsections, is occurring in the optically emitting gas.

iii) *Electron Density Derived from Radio Depolarization*

Figure 7 shows that the percentage linear polarization in the southwest ridge is about a factor of 3 lower at 1.49 GHz than at 4.86 GHz. There are various possibilities for the spatial distribution of ionized gas and magnetic field responsible for this depolarization (Burn 1966). If the depolarizing region were external to the synchrotron-emitting region, variations in Faraday rotation across the extent of the synthesized beam (beam depolarization) would be responsible. This arrangement seems unlikely since there is a strong correlation between depolarization and observed radio brightness, which suggests that the depolarizing gas is mixed together with the synchrotron-emitting region. In this case, the depolarization is produced by different amounts of Faraday rotation suffered by emitting regions spread out along the line of sight in the presence of an ordered field. In addition, there may be a contribution by randomly oriented fields producing beam depolarization.

The simplest internal depolarization model is that consisting of a uniform slab containing an ordered magnetic field component parallel to the line of sight. The synchrotron-emitting electrons and the Faraday rotating medium coincide. The observed degree of linear polarization at some wavelength where the total Faraday rotation through the slab is ψ and may be derived from equation (18) of (Burn 1966)

$$\frac{P}{P_i} = \frac{\sin(\psi)}{\psi}, \tag{5}$$

where P_i is the degree of linear polarization at zero wavelength. The quantity ψ is given by

$$\psi = 8.1 \times 10^5 n H_{\parallel} L \lambda^2 , \quad (6)$$

where n is the electron density, $H_{\parallel}$ is the parallel component of the (uniform) field, and L is the slab thickness.

Taking $P/P_i = 0.3$ in the ridge at 1.49 GHz ($\lambda = 0.2$ m) gives $\psi = 2.4$ rad. If the parallel magnetic field is taken to be the equipartition field in the ridge, and $L = 0.1$ pc, then $n = 10$ cm^{-3}. This density is probably an underestimate since there is no allowance for a component of the equipartition field orthogonal to the line of sight in this model. Note that this model predicts an observed rotation of the plane of polarization of $\psi/2$, or 1.2 rad, but unfortunately no comparison with observation can be made because of the galactic component of Faraday rotation.

A more realistic model for the depolarization corresponds to the geometry in Figure 13 in which the field has a component which extends radially outward from the center of the shell in addition to a totally disordered component. Adopting this picture, we model the source as a slab of emission extending along the line of sight symmetrically with respect to the position of the nova. The mean longitudinal component of the ordered field is zero, but there are components of opposite sign in the two halves of the slab. We let the radial (ordered) field be H_o and the random component of the field be H_r, and let it vary randomly on a linear scale d. The relative strength of the ordered and random components is determined approximately from the equation given by Burn (1966):

$$P_i = \frac{H_o^2}{(H_o^2 + H_r^2)} . \quad (7)$$

Here P_i is, as before, the degree of linear polarization in the high-frequency limit where Faraday effects are not important. If we take $P_i = 0.20$ estimated from the 4.9 GHz polarization map, we obtain $\beta \equiv H_r/H_o = 2.0$. This modified picture is a slightly more complex version of a simple slab model involving uniform and random magnetic field components analyzed by Burn (1966). By incorporating appropriate modifications, we find $n = 46$ cm^{-3}, if we use $H_o = 3.3 \times 10^{-5}$ G, derived from the equipartition field with $\beta = 2$. This result is rather insensitive to d in the range $0 < d/R < 0.1$, where R is the radius of the nova remnant.

This figure is probably more realistic than the previous estimate of 10 cm^{-3} since it is based on a more realistic model for the magnetic field geometry. However, in view of the uncertainty in this geometry, we prefer a more conservative conclusion that the mean electron density lies in the range $10 < n < 50$ cm^{-3}. It is the model dependence of the density that is the principal cause of its uncertainty. For comparison, an error of a factor of 2 in the measured depolarization ratio would introduce an error of only 20% in the derived electron density.

In order to estimate the shell mass, we note that its outer radius and width are, respectively, about 2.7×10^{17} cm and 1.0×10^{17} cm, and that the radio shell subtends a solid angle of 1.84 steradians at the star. The mass range corresponding to the above density range is then 1.5×10^{-4} to 7.4×10^{-4} $M_\odot$ allowing for a polar shell on the other side of the star. Since about 40% of this is material swept up (see § IV*d*), the mass of the material in the nova ejecta is 0.9×10^{-4} to 4.4×10^{-4} $M_\odot$. These figures would need to be approximately tripled if the ejecta shell were spherically symmetric. However, nova shells are not generally spherically symmetric, and this revision would be unjustified. Thus the inferred mass is the range appropriate for a typical nova shell.

If the depolarizing gas were identified with ambient gas heated by the forward shock wave, and in the absence of significant cooling (see § IV*c*), then its temperature would be about 10^7 K, and it would therefore be a source of X-ray emission. Assuming a thickness corresponding to the derived ridge thickness of 15″, and X-ray emissivities given by Raymond, Cox, and Smith (1976), the X-ray luminosity for a density of 46 cm^{-3} is 1.2×10^{33} ergs s^{-1}. The observed X-ray luminosity of GK Per in the quiescent state in the 0.15–4.5 keV range is about 1.3×10^{32} ergs s^{-1} (Becker and Marshall 1981), of which less than about 35% emerges from the nonstellar component (Cordova and Mason 1984). Thus the gas responsible for the depolarization is substantially cooler than the forward shock-heated component. This is consistent with its identification with cooler and denser ejecta represented by the spatially coincident blobs of optical emission (see § IV*c*).

iv) *The Radio Spectrum*

The turnover in the integrated radio spectrum at 1 GHz may be produced by several processes, namely (i) synchrotron self-absorption; (ii) cyclotron turnover; (iii) free-free absorption by internal ionized gas; (iv) the Razin effect (Razin 1960); (v) a bend in the energy distribution of the radiating electrons. Synchrotron self-absorption and cyclotron turnover can immediately be ruled out as the former requires a magnetic field strength of $\sim 10^{18}$ gauss and the latter requires that the radiating electrons stream out essentially along the magnetic field, at pitch angles $\sim 2 \times 10^{-7}$ rad (assuming the equipartition magnetic field). The emission measure required to produce a free-free optical depth of unity at 1 GHz if $T = 10^4$ K is 3×10^6 cm^{-6} pc. Such a high emission measure would produce a brightness temperature of about 400 K at 4.9 GHz, which is three orders of magnitude higher than the observed maximum brightness. Therefore free-free absorption is ruled out. The Razin effect combined with the equipartition magnetic field in the ridge requires an average electron density of 4×10^3 cm^{-3}. This is also impossible since the emission measure over any plausible path length would be even larger than that implied by free-free absorption.

Thus we conclude by elimination that the turnover is produced by a bend or low-energy cutoff in the energy spectrum of the emitting electrons. It is noteworthy that the age of the remnant is much smaller than the time scales (measured at the current epoch) for various particle energy loss mechanisms which could produce this bend, including synchrotron, inverse Compton, and ionization losses. We conclude therefore that the electron energy spectrum is that produced by the acceleration process itself, and hence it contains in principle information about the process of shock acceleration. We return to this point later.

The spectral index map in Figure 8 shows that the spectral index is consistent with nonthermal emission throughout the remnant. Though there appear to be spatial variations in the spectral index, these are by and large attributable to noise. A possible exception is a gradient in the spectral index at the bright ridge in the sense that steeper spectra occur nearer to the edge. This variation appears to be significant, but there is no apparent physical cause.

v) *Conditions in the Optical Knots*

Figures 10 and 11 (Plates 18–20) show that the GK Per shell has evolved optically into a series of knots, seen most

PLATE 18

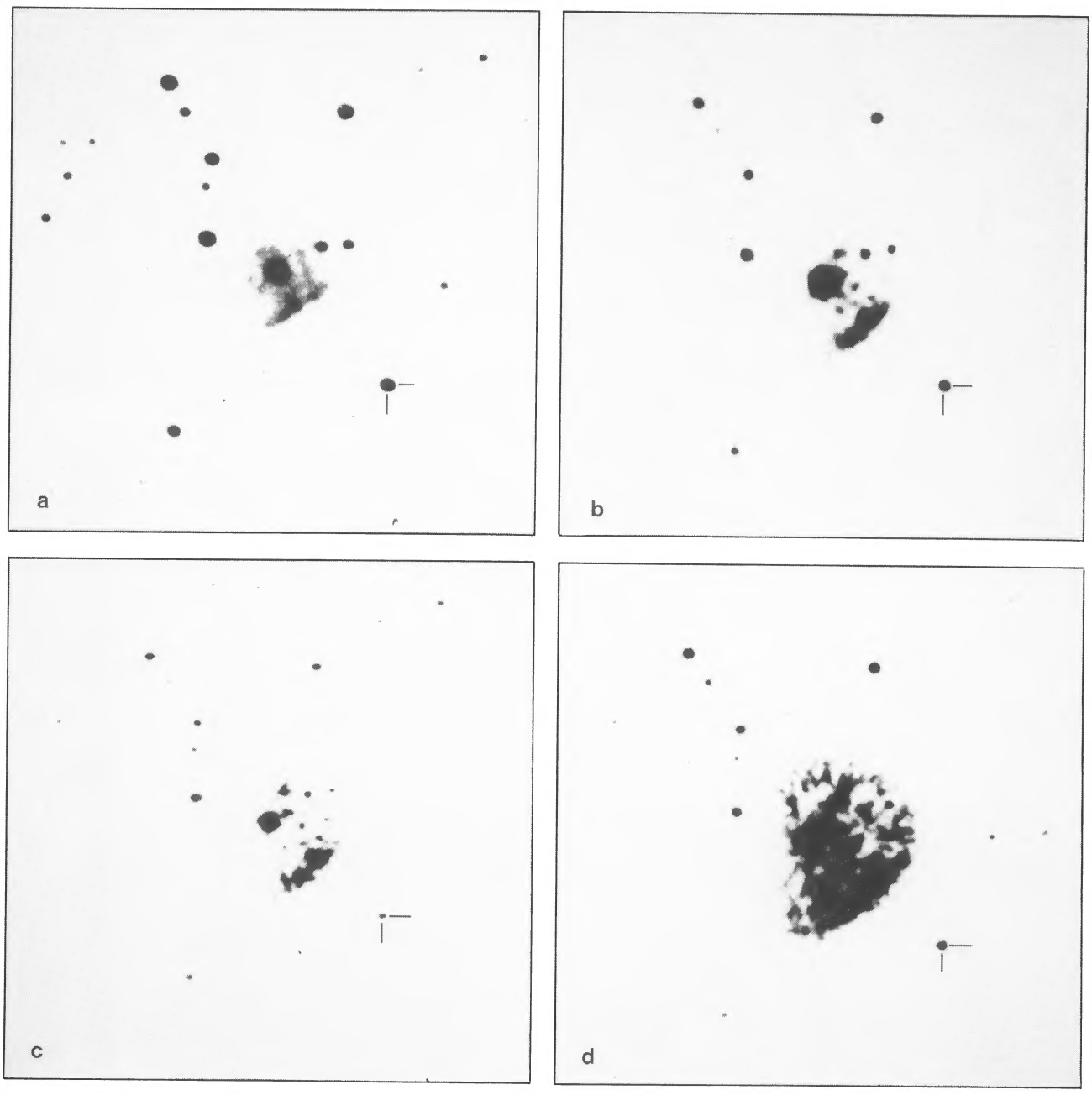

FIG. 10*a–d*

FIG. 10.—Photographs of the expanding ejecta of GK Per, taken (*a*) 1917 Nov. 15, (*b*) 1937 Oct. 6, (*c*) 1942 Nov. 6, (*d*) 1944 Oct. 15, (*e*) 1949 Nov. 20, (*f*) 1959 Dec. 19, (*g*) 1972 Sep. 8, (*h*) 1977 Nov. 16 (see Table 4 for further details). The reference star marked in all frames is 43″ from the nova.

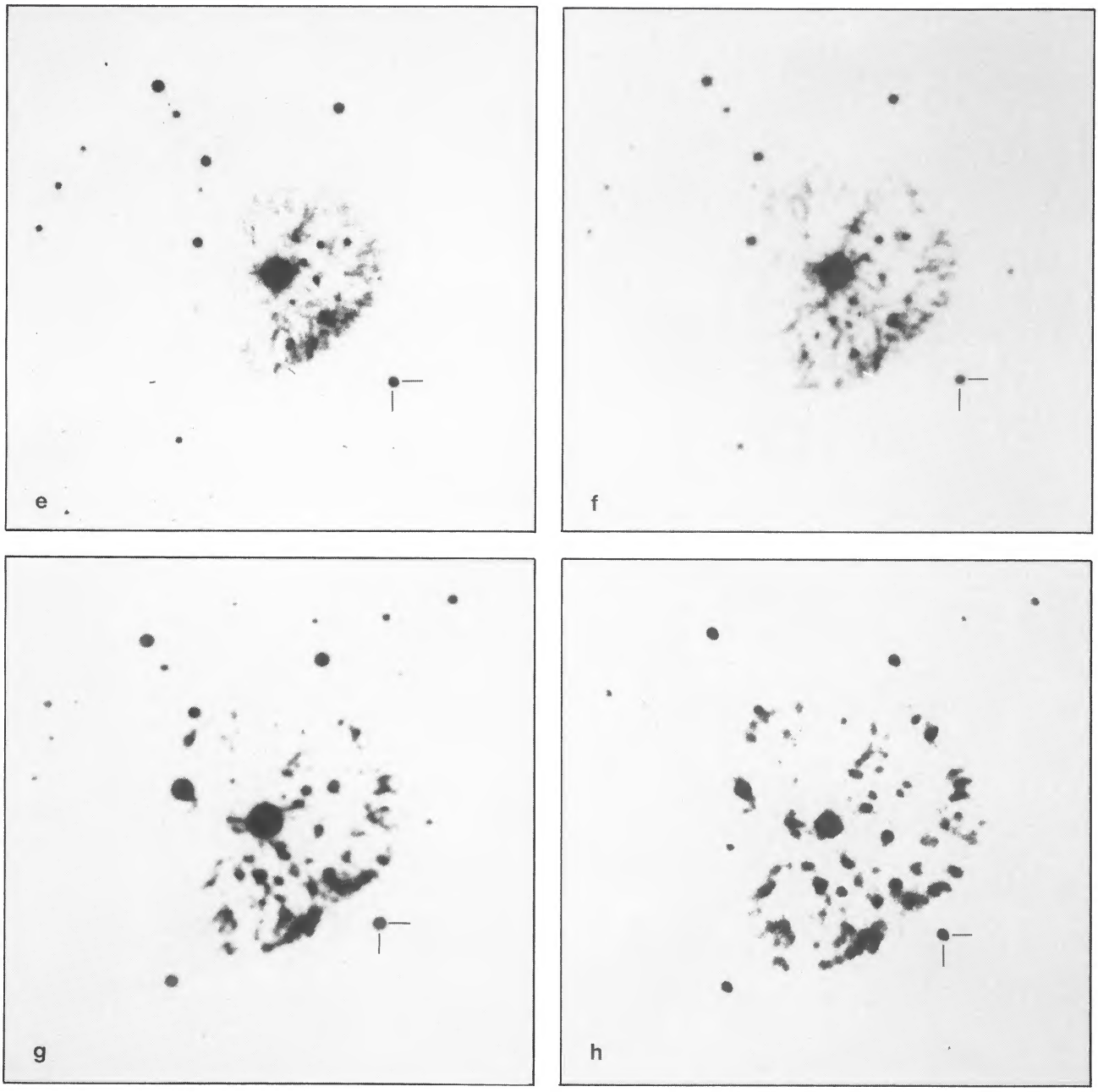

FIG. 10*e–h*

SEAQUIST *et al.* (*see* **344**, 818)

PLATE 20

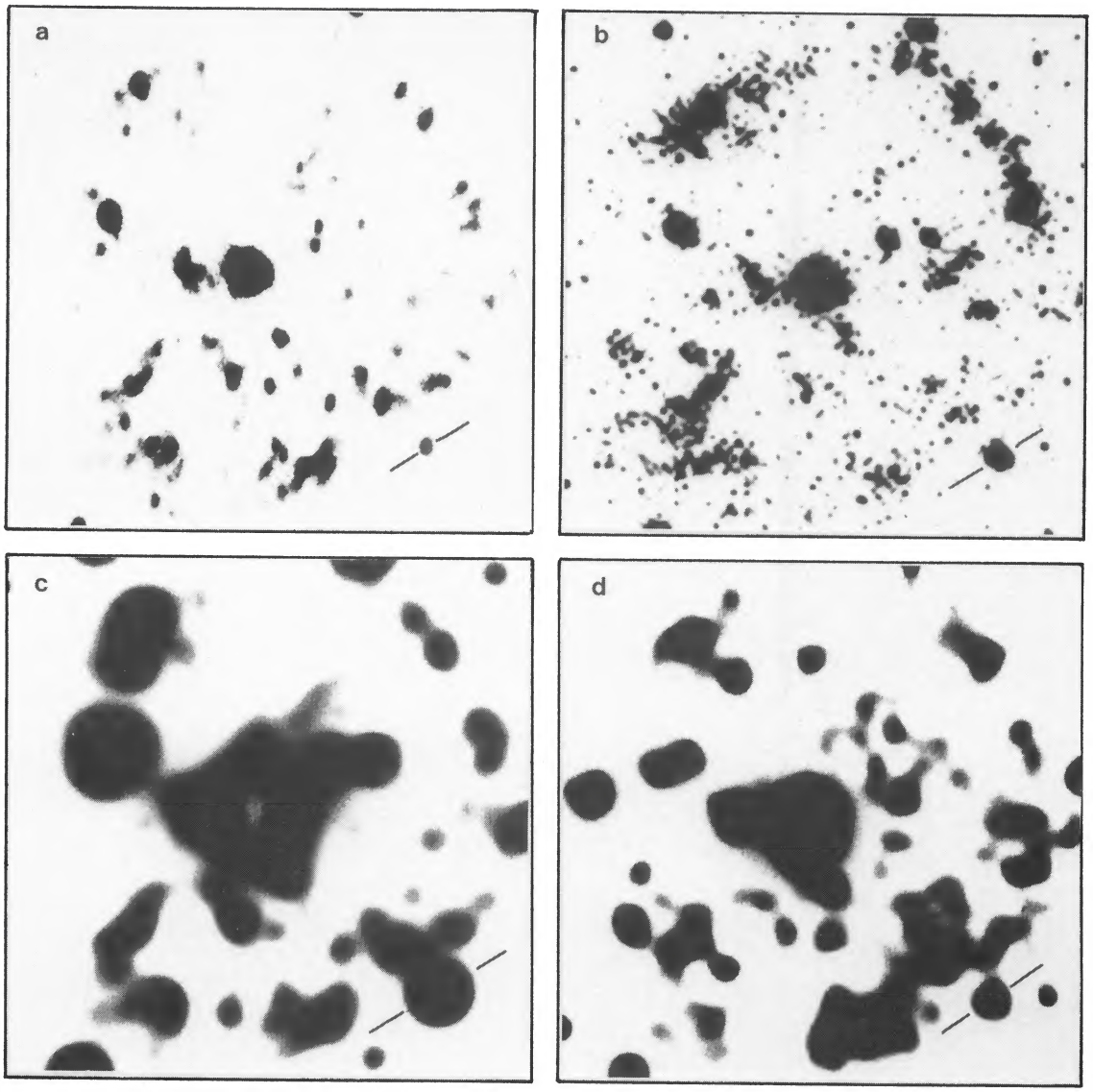

FIG. 11.—CCD images of the ejecta of GK Per taken through (*a*) an [N II]/Hα filter (1984), (*b*) [O III] filter (1986), (*c*) *R* filter (1987), and (*d*) [O II] filter (1987) (see Table 5 for further details).

clearly in [N II]. No radio emission is detectable from the individual knots, although the density of knots is highest within the bright radio-emitting region. The lack of detailed correspondence between radio and optical emission suggests an upper limit of about 0.1 K in the brightness due to free-free emission from individual knots. This limit in turn leads to the limit $n^2\phi^3 < 4 \times 10^7$ cm^{-6} arcsec^3, where ϕ is the angular diameter of a typical knot. An electron temperature of 10^4 K is assumed. From the critical density of the upper state of the [N II] λ6584 transition, we must also have $n < 10^5$ cm^{-3} in the knots. An even stronger limit of less than 3×10^3 cm^{-3} applies to the [O II] λ3729 line emission (the stronger line of the doublet) which we have demonstrated to be cospatial with [N II] λ6584 by blinking the images. Note that the northeastern portion of the remnant is relatively devoid of both knot emission and radio emission.

It may also be seen from a comparison of images in Figure 11 (Plate 20) that the knots in [N II], [O II], and [O III] generally coincide except for the radio-emitting ridge. In the ridge there is an absence of [O III] emission in the knots, where [N II] and [O II] are bright, which yields further information on the conditions in the knots in the ridge. Seitter and Duerbeck (1987) have also noted the different distributions of [N II] and [O III] in GK Per and RR Pic, and Seitter (1985) has suggested that in the latter case, the differences are caused by changes in abundance across the remnant. We return to this point in § IV*c*.

c) Physical Processes in the Interaction Region

The picture we adopt here is similar to that of a young SNR in the pre-Sedov phase (e.g., Chevalier 1977*a*). There is a contact discontinuity separating the ejecta from the ambient upstream gas. Ahead of this boundary, there is a shock propagating through the ambient medium. There is also a reverse shock propagating in the downstream sense into the ejecta.

i) *Postshock Region*

With a forward shock speed of approximately 1000 km s^{-1}, the temperature of the gas immediately behind the shock is of order 10^7 K as noted in § IV*b*, and the density roughly 4 times that in the preshock region. Later, we conclude that the preshock gas has a density of about 0.8 cm^{-3}, so that the shocked gas density would be 3 cm^{-3}. If the gas cools appreciably, then the temperature drops and the density rises significantly. The strongest emission line in the remnant is due to [N II] which has a luminosity of 7.5×10^{32} ergs s^{-1} with an uncertainty of about an order of magnitude (Duerbeck 1987*a*). This is much lower than the rate of energy input to the shock region ($\sim 10^{35}$ ergs s^{-1}), and we conclude that radiative cooling is unimportant. Consequently the shock is adiabatic. This conclusion may be derived independently by comparing the cooling time ($\sim 10^4$ yr) with the age of the remnant ($\sim 10^2$ yr). Therefore the density and temperature in the postshock region will remain at, respectively, 3 cm^{-3} and 10^7 K. The width of the forward shocked region should be about $\frac{1}{4}$ the radius of the shell, or about 10″. This is in reasonable agreement with the derived thickness of the radio-emitting ridge (15″). Moreover, these conditions would yield an X-ray luminosity about two orders of magnitude lower than the estimate based on the density derived from Faraday depolarization, and hence is compatible with the upper limit by Cordova and Mason referred to in § IV*b*.

The foregoing result, coupled with the results of the Faraday depolarization analysis, and the appearance of blobs in the emission lines of [N II] and [O III], show that the remnant is very inhomogeneous in both density and temperature. A possible reason is the fragmentation of the ejecta by Rayleigh-Taylor instabilities originating at the contact discontinuity, as illustrated in Figure 13. The archival photographs in Figure 10 (Plates 18–19) show that the knots have grown in prominence, beginning some time before 1949, suggesting the growth of these instabilities. Although there is no direct evidence that the knots in GK Per, or similar knots in Cas A arise from this process, there is theoretical support for its occurrence during the transition to the Sedov phase (Gull 1975; Jones, Smith, and Stroka 1981). GK Per is in this transition phase, which is characterized by a deceleration of the ejecta as a comparable mass is swept up (see § IV*d*).

To investigate this point further we examine the conditions in the knots in more detail. It was noted in § IV*b* that in regions where there is no radio emission, the [N II] and [O III] emission is strongly correlated. However, in the radio-emitting zone, very little [O III] emission is seen, even though [N II] is very strong. This absence must reflect a spatial variation in conditions within the knots rather than in chemical abundance since [N II] and [O II] are both strong in the shock region. The ionization within the knots is determined by the speed of the reverse shock propagating into the nova ejecta. Cox and Raymond (1985) have shown that the ratio [O III]/[O II], and by inference the ratio [O III]/[N II], is very sensitive to shock velocity. The [O III] emission is strongly suppressed at shock speeds below 100 km s^{-1}. Thus the reverse shock in the ejecta within the radio-emitting region must have speed less than 100 km s^{-1}, at least an order of magnitude less than the forward shock speed. Since the shock velocity varies inversely as the square root of the density, the density within the brightest [N II] knots is at least two orders of magnitude higher than the ambient value, i.e., $n > 100$ cm^{-3}. With these higher densities, cooling will be important and the kinetic temperature will be close to 10^4 K. In this case, equilibrium with the mean pressure in the hot postshock environment suggests a density in the blobs of about 2×10^3 cm^{-3}. From the limit set by the absence of free-free emission from these blobs discussed in § IV*b*, the angular diameter of these regions must be less than 1″.6, in agreement with observation. In the non–radio-emitting region, where [O III] is detected in the blobs, the shock speeds are presumably higher and the densities much lower.

We conclude that the Faraday depolarization is probably produced by the cooler dense blobs associated with the nova ejecta. This conclusion is strongly supported by the spatial coincidence between the region of maximum depolarization and maximum knot density. If the mean density from depolarization arguments is 10–50 cm^{-3}, and the blob densities are near 2000 cm^{-3} then the volume filling factor f of cool gas in the depolarizing region is in the range 0.5%–3%.

A very important constraint on the rms electron density in the region of depolarization may be derived from the apparent absence of radio free-free emission. Figure 8 shows clearly that the spectral index steepens in this region rather than flattens, as would be expected if thermal emission were making a contribution. A very conservative upper limit to the level of thermal emission would be 0.5 K in the beam-averaged brightness temperature, roughly the maximum observed brightness in the ridge at 4.86 GHz. The corresponding upper limit on the optical depth at this frequency is 5×10^{-5} assuming an electron temperature of 10^4 K. With a path length of 0.1 pc, this

yields $n_{rms} < 200$ cm^{-3}. Since $n_{rms}/n_{mean} = f^{-1/2}$, then if we adopt $n_{mean} > 10$ cm^{-3} to obtain $f > 0.3\%$ in agreement with the above estimate.

ii) *Origin of the Magnetic Field*

It is probable that the magnetic field in the remnant is amplified by turbulence originating from Rayleigh-Taylor instabilities in the decelerating ejecta, similar to that which may occur in supernova remnants (see, e.g., Chevalier 1977*a*; Kulsrud *et al.* 1965; Gull 1975). This effect could equally well account for the radial field directions observed. The seed field in the preshocked gas could be either a preexisting interstellar field, or a circumstellar field, originating with the star. Considering the latter case, the field may be dragged out from the white dwarf by the ejecta. If the dependence on radius of the unamplified (seed) field is r^{-2}, appropriate for a radial field configuration, and the seed field is scaled by this law to the radius of a white dwarf (10^8–10^9 cm), then the surface field on the white dwarf would be $(5 \times 10^{12}$–$5 \times 10^{14})\eta$ gauss, where η is the ratio of the seed to the observed equipartition field. This is much too high unless $\eta \leq 10^{-6}$. A dependence of the form $1/r$, appropriate for a tightly wrapped field would yield $(2 \times 10^4$–$2 \times 10^5)\eta$ gauss, where the latter figure applicable for a high mass WD, is in line with the field strength deduced by Bianchini and Sabbadin (1983) to account for the hard X-ray emission from GK Per.

iii) *Relativistic Particle Acceleration*

As was noted earlier, the efficiency of relativistic particle production is similar to that in SNRs. This fact, combined with the morphological similarities in the radio with young SNRs, indicates that the basic acceleration processes may be identical despite a difference of six orders of magnitude in overall energy scale. The synchrotron-emitting ridge coincides with the brightest [N II] knots in the southwest ridge. This is consistent with recent numerical computations by Dickel, Eilek, and Jones (1988) which show that relativistic particles are accelerated by hydromagnetic turbulence generated in the Rayleigh-Taylor unstable regions. This process is augmented by first-order Fermi acceleration at the shock boundaries. The synchrotron-emitting ridge should occupy the region between the forward and reverse shocks.

The radio spectrum in Figure 4 shows that the electron energy spectrum is curved rather than strictly power-law over the energy regime sampled. Unfortunately, too little is known yet about the details of the acceleration process to make any comparison with theory. Both turbulent acceleration and shock acceleration processes may give rise to departures from power-law spectra (Schlickeiser 1986; Takahara 1986; Dickel, Eilek, and Jones 1988). In the future, our result should provide a key constraint in understanding the particle acceleration processes in nova and supernova shells.

d) A Simple Model for the Shock and Its Evolution

The nonthermal radio emission, and its association with a flattened portion of the optical image of the remnant, signify clearly that the nova ejecta are interacting primarily with an ambient medium located to the southwest of the nova. The earliest evidence for this interaction is in the image for epoch 1917 (see Fig. 10 [Pls. 18–19]. A luminous feature parallel to the flattened ridge of the currently observed shell is apparent in the southwest quadrant, probably indicating the development of a shock front. The site of this ambient material is in the same direction relative to the nova as the material responsible for the light echo, but is much closer to the star, and must have a lower density (see § IV*a*[iii]). A polar cone geometry for this material is suggested by the observation that the angle subtended at the star by the flattened interaction zone is remarkably constant (about 90°) among all of the archival photographs later than 1917. If a spherical shell encountered a plane-parallel slab of material, this angle would steadily increase with time, unless the slab were very thin producing an impulsive interaction. The latter picture is ruled out by the span of time involving the interaction, ranging from 1917 to the present when there is evidence that the shell is still slowing down (see Fig. 14). A continuous interaction with a polar cone, however, is consistent with the observed behavior since the

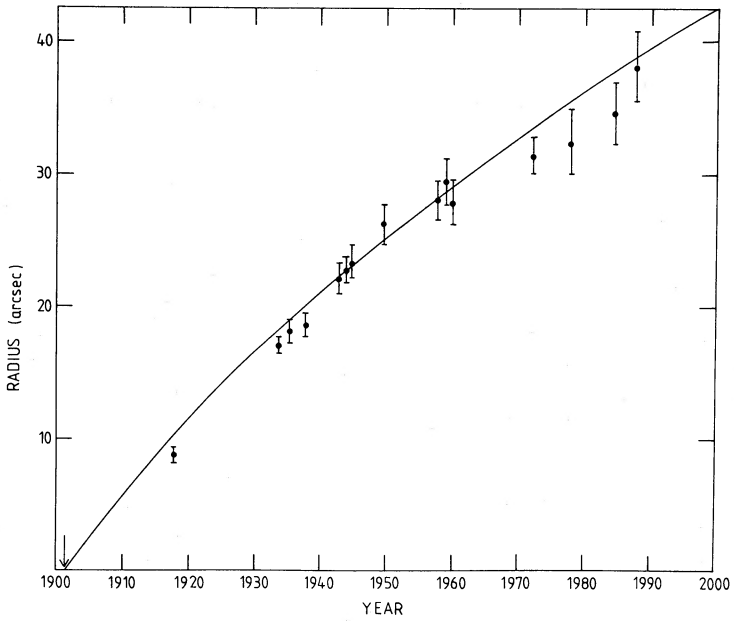

FIG. 14.—The variation with time of the optical radius of the GK Per remnant measured in a direction perpendicular to the bright radio ridge. The smooth curve corresponds to a least squares fit for a simple model conserving energy in the shock.

angle subtended at the star by the interaction zone would be just the (constant) angle subtended by the cone itself. If the PN picture, discussed in more detail below, is correct, then the existence of circumstellar material with this geometry would seem to suggest that the nova ejecta are interacting with a part of the PN not directly associated with the proposed IR emitting torus. It may, however, be related to the light echo region farther out, as discussed in § IV*e*. This region may be significantly less dense than the torus, and represent a separate feature of the PN. If it is a fast wind following the ejection of the main shell, then its velocity must be considerably less than 1000 km s^{-1} to permit the observed shock interaction with the nova ejecta. Its polar cone geometry may be the result of modification by the toroidal geometry of the main shell ejected. The onset of the interaction in 1917 may signify the collision between the nova ejecta and the inner edge of the polar cone marking the end of this phase of ejection.

To investigate this picture further, we have used the proper motions derived from the archival images to determine the time dependence of the radius of the shell in the southwest quadrant. We have compared this result with simple momentum conserving and energy conserving models for the shock interactions between the nova shell and an ambient medium comprising two oppositely directed polar cones of gas whose axes are aligned perpendicular to the orientation of the shock wave. For reasons discussed in § IV*e* we assume a mass density distribution in the polar cones of the form

$$\rho = \frac{A_p}{r^2}, \tag{8}$$

which implies a steady mass outflow at constant speed (V_p) during the period of ejection of these cones. We treat the interaction as a collision between a piston representing the nova ejecta and the above density distribution. This analysis ignores the break up of the nova ejecta by Rayleigh-Taylor instabilities, and consequently the results must be treated cautiously. However, a more complex analysis is beyond the scope of this paper, and possibly unjustified before more information on the shock conditions is available. In our simplified model a shock wave forms in front of the slab whose properties depend upon whether or not the shock is isothermal (i.e., whether there is rapid cooling behind the shock) or whether it is adiabatic (cooling unimportant). In the first case, it is appropriate to treat the motion of the slab by conserving momentum, and in the second case by conserving energy (see Kaplan 1966). In the first case the result for the radius r in terms of time t is

$$r = \beta_m\left(\sqrt{1 + \frac{2v_0 t}{\beta_m}} - 1\right), \tag{9}$$

where $\beta_m = M/4\pi A_p$, M is the mass of the ejecta, and v_0 is the initial velocity of the ejecta.

In the second case, the result is

$$r = \beta_e\left[\left(1 + \frac{1.5v_0 t}{\beta_e}\right)^{2/3} - 1\right], \tag{10}$$

where $\beta_e = M/4\pi A_p \eta$, and η is the ratio of total energy (including internal energy) to outflow kinetic energy in the shocked region.

Figure 14 shows a plot of the measured radius versus time for the southwest quadrant with a theoretical curve for the adiabatic shock. A value of $\eta = 2$, appropriate for a strong adiabatic shock, was used. Both the isothermal and adiabatic cases give an acceptable fit to the measurements, yielding the following results:

Isothermal case:

$$A_p = 6.9 \times 10^{10}(M/10^{-4}\ M_\odot)\ \text{g cm}^{-1} \quad v_0 = 1600\ \text{km s}^{-1}.$$

Adiabatic case: (11)

$$A_p = 1.1 \times 10^{11}(M/10^{-4}\ M_\odot)\ \text{g cm}^{-1} \quad v_0 = 1700\ \text{km s}^{-1}.$$

If the mass of the nova ejecta is $10^{-4}\ M_\odot$, typical of that for other novae (Seaquist 1989), then equation (11) for the adiabatic case leads to a density at $r = 2.7 \times 10^{17}$ cm (the current radius) of about 0.8 cm^{-3} for the preshock medium, and a mass for the polar cone swept up of about $6 \times 10^{-5}\ M_\odot$. Here the angle subtended by the cone has been assumed to be 90°. The inferred mass outflow rate is 1.3×10^{-7} (V_p/100 km s^{-1}) $M_\odot$ yr^{-1} allowing for a second cone in the northeast quadrant.

The model presented above for the shell interaction does not account for the obvious asymmetry between the northeast and southwest quadrants. No comparable interaction zone is detected in the radio toward the northeast. Some asymmetry in the nova shell must in any event be invoked to account for the lack of optical emission on the eastern side of the remnant on all archival photographs. It is unclear whether the mass of ejected material is lower in this direction or whether the distribution of ambient material is asymmetric. It is worth noting in the latter context that the light echo also exhibited a distinct preference for the southwest quadrant.

The assumed geometry for the interacting medium may not be the only picture leading to a successful quantitative description of the evolution of the nova shell and the characteristics of the radio-emitting shock. However, the polar cones with an inverse square law density profile have another attractive feature which relates to the existence of the light echo produced by a slab of material about one parsec to the southwest of the nova. We discuss this relationship next.

e) The Relationship of the Interacting Medium to the Light Echo Region

It is particularly significant that the direction of the light echo, the axis of the *IRAS* bipolar nebula, the alignment of the H I emitting cloud, and the alignment of the shock wave are either parallel or orthogonal. This is especially noteworthy given that the distance from the nova to the shock is at least one order of magnitude smaller than the scale of the other features.

This alignment over a wide range in scale is satisfied by the assumption that the polar cones discussed in the previous subsection are associated with a PN. Consider the following picture. During the formation of the PN, the ejection of the toroidal shell was accompanied by a less massive but continuous outflow of material along the axis of the torus. This outflow formed the two polar cones, and in addition swept up preexisting interstellar or circular stellar gas. This action would form a concentration of material, or a shell of gas and dust, at the radius of the proposed light echo. The weaker *IRAS* emission detected in both directions along the axis of the proposed toroid may also be related to this swept-up material. This shell is shown in Figure 13. A quantitative analysis of this picture is presented in Appendix I. We assume in Appendix I that the slab of light echo material is gas and dust from the earlier red

giant wind, swept up by the polar cones. It is shown there that a self-consistent picture can be constructed provided that the polar cones possess an outflow velocity of about 200 km s^{-1} and a mass-loss rate about two orders of magnitude lower than that of the main PN shell. In particular, the mass swept up in the light echo region would be about 10^{-1} $M_\odot$ for a red giant mass-loss rate of about 10^{-5} $M_\odot$ yr^{-1}. This mass is compatible with the amount of dust about 10^{-3} $M_\odot$) required to account for the light echo.

We conclude that the observed circumstellar phenomena associated with GK Per are consistent with an ancient PN. We stress, however, that the data so far do not preclude alternative interpretations. In this regard we note that Hessman (1988) finds that the CO distribution is asymmetric and that the mass of molecular gas bounded by the *IRAS* emission is 2 $M_\odot$ (uncertain to within an order of magnitude). He notes that these factors, as well as the asymmetry of the light echos, cast doubt on the stellar origin for *all* of the material detected in the vicinity of GK Per. We concur that the picture is far from tidy, and that some of the features of the environment could have an interstellar origin.

f) GK Per and Cataclysmic Variable Evolution

Our initial interpretation of the discovery by Reynolds and Chevalier (1984) that GK Per is a nonthermal radio source, with obvious similarities to young supernova remnants, was that the ejecta were running into an interstellar cloud that happened to lie in close proximity to the nova. The search for this cloud led to the discovery of the H I and *IRAS* nebulosities which are striking in their symmetrical placement about the nova. This, and their alignments with the central radio ridge, and light echo material, have led us to question the interpretation purely in terms of some random proximity. As outlined in Bode *et al.* (1987), and Seaquist *et al.* (1988), the implied morphology, size, expansion velocity and mass of the H I/*IRAS* nebulosity, are compatible with those of a PN composed of neutral material. In this sense then it might be termed a "fossil" PN. In this section we discuss the stellar data which bear on the PN interpretation.

First we will consider the more circumstantial evidence in favor of the PN picture. We know that GK Per contains a short-period binary comprising a massive white dwarf and an evolved K-type subgiant in an orbit with around a 2 day period (see § I). Obviously, somewhere in the formation process of the white dwarf a PN was shed. Balick (1987) has reviewed the association of the morphologies of planetaries with the central stellar systems. He finds that bipolar morphology is associated with planetaries expelled from short-period binary systems, such as the one we have here. The detailed reasons may be linked to the lower effective gravity in the plane of the binary orbit. It is then of interest to note that GK Per is of high inclination (§ I). The mass implied from the H I observations is in line with that for the more extended, massive PN, associated with massive stars (Pottasch 1980; Barlow 1987).

The question of the formation of CV systems in general has been considered by several authors (see Webbink 1985 for a review). It was originally suggested that the progenitor of such systems might be W UMa binaries as their angular momenta are similar to CVs. However, as pointed out by Ritter (1976), angular momentum loss is required to form systems with the very short orbital periods found among CV binaries. Such loss can occur during a common envelope phase during which a large amount of mass is shed from the system. Meyer and Meyer-Hoffmeister (1979) have considered in detail the evolution of a binary with initial separation of several hundred solar radii, in which the primary star enters a red giant phase, enveloping the companion (main-sequence star) in a common envelope in which the degenerate core of the giant and the main-sequence star now form the effective binary system. The frictional drag experienced within this envelope decreases the binary separation and puts energy into the common envelope. Over a time scale of around 1000 years the binary period becomes comparable to that seen in CV systems. Around the time when the outer layers of the secondary star are affected by the tidal interaction, a large amount of mass may suddenly be lost from the common envelope and the neighborhood of the degenerate primary. The sudden increase in luminosity in the central regions of the common envelope would then lead to expulsion of the envelope to reveal the close binary, which in many ways would resemble a CV system. The Meyer and Meyer-Hoffmeister models follow the evolution to just before this last phase and did not produce mass ejection as the core-main-sequence binary was corotating with the region around it. Detailed three-dimensional modeling by Livio and Soker (1988), where none of the envelope is necessarily corotating, has led to mass ejection which is much enhanced in the equatorial regions, particularly when the primary envelope is that of a red giant, rather than a supergiant.

In support of these models, as remarked earlier, several PN contain short-period binaries. These include UU Sge (Bond, Liller, and Mannery 1978), and the ultra short-period binary ($P = 2.72$ hr) at the center of Abell 41, referred to as a precataclysmic binary (Grauer and Bond 1983). Of even greater interest is the controversial object V605 Aql (Nova Aql 1919) which lies toward the center of the PN Abel 58 (van den Bergh 1971; Duerbeck 1987*b*). This has been classified as a very slow nova, but its real status is still uncertain.

If indeed we are seeing the PN associated with expulsion following the common-envelope (CE) phase of the central binary in GK Per, it is then possible to estimate its age. The H I line width shows little evidence for velocities in excess of 5 km s^{-1} (see § III*b*). This low velocity is in line with those of the largest PN whose dimensions are of order a few tenths of a pc at $z < 150$ pc from the Galactic plane (Geiseking, Hippelein, and Weinberger 1986), note GK Per lies at $z < 80$ pc). Typical values of expansion velocity for young, more compact objects are around 20 km s^{-1}. The mechanism for deceleration is poorly understood, but it is most likely related to interaction with an earlier mass-loss phase (Sabbadin *et al.* 1984) similar to that suggested for the polar cones. With toroidal radius around 2×10^{18} cm a minimum expansion age of $t_0 = 3 \times 10^4$ yr results. The maximum age is more poorly defined because we have only an upper limit to the current expansion velocity, but taking a value of 5 km s^{-1} gives this limit as $t_0 = 1.3 \times 10^5$ yr.

There is one potentially serious problem with the PN picture. Paczyński (1971) has computed evolutionary tracks for the central stars of PN (CPN) with masses 0.6, 0.8, and 1.2 $M_\odot$. If the estimates of Bianchini and Sabbadin (1983) are correct, then the total luminosity of the central system GK Per is around 2×10^{34} ergs s^{-1}, much of which must be associated with the accretion disk. Thus the white dwarf luminosity may be only of order $L_\odot$. From the Paczyński models it would appear that we would require the white dwarf to lie at the top end of the published mass range if such a low-luminosity white dwarf is to be formed on the required time scale. More recently

Iben and Tutukov (1984) have computed the luminosity evolution of a 0.6 $M_\odot$ CPN and at $t = 10^5$ yr find L approximately 50 $L_\odot$. An increase of mass of the CPN on this model requires a longer time to decrease to the same luminosity, thus yielding a conflict either with the deduced mass of the white dwarf, or the derived age of the remnant.

There are however several unknowns and uncertainties here. First, Bianchini and Sabbadin (1983) have used a very low value of $E(B-V)$ $(=0.1)$ to correct their UV data for interstellar extinction. Using the more likely value of $E(B-V) = 0.3$ (Wu *et al.* 1989; Roberts *et al.* 1988), the corrected monochromatic UV fluxes would be consistent with the expectations of Iben and Tutukov if the blackbody temperature of the white dwarf were in excess of 10^5 K. However, this still neglects the fact that much of the UV flux must arise from the accretion disk. Second, the upper limit to the expansion age is rather ill-defined for the reasons given above. Finally, the evolutionary history of the central star of a PN formed in a common-envelope interaction is likely to be rather different from that of a single star. Certainly, the assumption that the common envelope is shed when the primary is at the tip of its AGB evolution is unlikely to be correct, bearing in mind the 1000 yr time scale for the CE phase. Thus the initial core conditions, including luminosity and temperature, will be very different from those assumed as the starting point of single-star CPN models. This whole area of work must be one of great interest, but presumably can be adequately explored only once the CE phase itself is better understood.

That GK Per is a relatively young nova is evident from its long orbital period as magnetic braking (and gravitational radiation) will decrease orbital periods during the V phase. Similarly, if the orbit is indeed elliptical (although this has been called into question by Crampton, Cowley, and Fisher 1986), this argues for youth as the circularization time of the orbit is likely to be short (King 1988). In addition to these points, the interaction of the ejecta with a surrounding medium suggests that the 1901 outburst may have been the first. We note here that Bode and Evans (1980) have estimated that a first-time nova in our Galaxy will be observed every $\sim$1000 yr (taking extinction, etc., into account). This further emphasizes the unique place that GK Per has in our understanding of these systems. Obviously, the ejecta are not presently in contact with material in the toroid, but are sweeping up matter which appears to be associated with the light echos, and most probably is in the form of a cone. This material in turn may be associated with a residual outflow or wind that accompanied the ejection of the main envelope in PN formation. In this connection, it has been suggested above that the enhanced magnetic field in the interaction region stems from the tightly wrapped field of the white dwarf itself.

The one-sided nature of this interaction could be due to a flow which is itself one-sided and may owe its origin to the impact of accretion modified by the magnetic field of the white dwarf, onto only part of the white dwarf surface. On the other hand, we may already be beginning to see evidence of an interaction in the northeast quadrant of the inner nebulosity.

If we have indeed discovered a PN associated with the ejection following the common-envelope phase of evolution of a CV, then GK Per will undoubtedly give a valuable insight into CV evolution. As we know so many parameters of the system, including a good estimate for the all important distance, this object may also prove invaluable for probing the longer term evolution of PN in general.

V. CONCLUSIONS

The results and analysis presented in this paper shed new light on the nature of the nova remnant GK Persei. This classical nova has many unique features, including a bright nonthermal radio shell, a rapid deceleration of its ejecta, the development of flocculent features in the ejecta, an unusually long orbital period, and (possibly) an unusually eccentric orbit. The nova is found to reside in the saddle of a bipolar nebula detected in the far-IR with *IRAS*. There is an associated H I feature showing a similar alignment. The alignment of these nebulae is parallel to the flattened portion of the nova shell representing the zone of interaction between the ejecta and circumstellar or interstellar gas to the southwest of the nova. This alignment is orthogonal to the direction from the nova toward the light echo detected shortly after the outburst. These observations suggest, but do not demonstrate conclusively, that the nova occurred in associated circumstellar material which is then most plausibly identified as an ancient PN with an age of about 10^5 yr.

We have explored the physical conditions in the nova environment with a view to examining the PN hypothesis. The optical and emission-line images, and the archival photographs of the gaseous remnant, lead to the conclusion that the interaction is very similar to that in a supernova remnant, even though the total energy involved is six orders of magnitude smaller. The angle subtended at the nova by the SW interaction zone is constant over a period comparable to the age of the nova, suggesting that the interacting circumstellar gas is confined to a polar cone whose axis is perpendicular to the axis of the bipolar nebula, and whose opening angle is about 90°. Simple energy conserving and momentum conserving models for the shock interaction with a polar cone yield a mass of 6×10^{-5} $M_\odot$ swept up by the expanding nova ejecta. If the proposed polar cone in this region is interpreted as part of the PN, it possesses a mass four orders of magnitude lower than that in the main shell.

A geometrical model of the main light echo shows that it was produced by a slab of material containing about 10^{-3} $M_\odot$ of dust located at a distance of about 1.4 pc from the nova. If it is assumed that this is the earlier red giant wind swept up by the polar cone ejected by the PN, then its gaseous mass would be about 10^{-1} $M_\odot$, yielding a plausible dust/gas ratio. A model for the polar cone based on this idea suggests that the cones have an outflow speed of about 200 km s^{-1}, much lower than the fast wind believed to emanate from some planetaries.

Much of the foregoing analysis supports the view that GK Persei exploded into its own PN, accounting for its unique characteristics. Figure 13 shows the spatial relationships among the various features discussed and conveys our PN picture. However, there are also a number of difficulties with this picture. The asymmetry of the expanding shell is not readily explained without invoking an asymmetry in either the nova explosion or the ejection of the PN shell. The age of 10^5 yr estimated for the PN, coupled with the theory of an isolated cooling white dwarf, requires a higher luminosity than the upper limit set by observations for the white dwarf primary. The interstellar medium in the region of GK Per has a complex structure, making it difficult to conclude in a definitive way that the *IRAS* and H I features are circumstellar rather than interstellar.

We intend to continue observations to further refine our knowledge of the physical parameters in the ejection region

and the circumstellar shell. These include observations in the radio continuum to measure the proper motion of radio knots, observations of [Fe II], [S II], and other lines to determine the conditions in the knots, and observations of CO to extend our knowledge of the temperature, density, mass, and motion of the H_2 in the circumstellar environment.

We thank Dr. H. W. Duerbeck for providing CCD images and spectral data, Dr. Rick Hessman for useful discussions and copies of the Yerkes plates, and Dr. K. Kamper for copies of archival plates. J. A. R. acknowledges the hospitality of Professor W. Seitter and the Institute for Astronomy, University of Münster, where PDS scans of the images of the reflection nebulosity were made. We would also like to thank warmly our colleagues at MRAO Cambridge, particularly Mrs. Sally Hales, Mrs. Teresa Michalik, and Dr. Julia Riley, for carrying out the OMT observations; and also Mr. Peter Warner and Dr. John Baldwin for giving us the CLFST data in advance of publication. Furthermore, we thank Mr K. Robinson for photographic work, Mrs. H. C. Poulton for line drawings, Drs. P. M. Allan and D. Ward-Thompson for help with STARLINK software, Dr. W. Martin and colleagues at the RGO for providing INT service time observations, and Dianna Larson of the Lick photo labs for provision of copies of archival material. We have had several useful discussion with Drs. M. Barlow, R. Braun, H. W. Duerbeck, and Professor W. Seitter. Dr. S. van den Bergh drew our attention to his work on V605 Aql. This research was supported by a grant to E. R. S. and a scholarship to D. A. F. both from the Natural Sciences and Engineering Research Council of Canada. M. F. B. is supported by a UK SERC Advanced Fellowship and J. A. R. by a National Advisory Body Research Assistantship. M. F. B. acknowledges the provision of travel funds by the UK SERC. J. S. A. is supported by the UK SERC.

APPENDIX A

A MODEL FOR THE FORMATION OF THE LIGHT ECHO SLAB

The polar cones are modeled as a steady outflow at constant velocity V_p with density dependence given by equation (8). We assume that the cones sweep up material originating from the earlier mass loss from the red giant precursor to the white dwarf. The red giant wind also has an inverse square density profile with density parameter A_g, and wind speed V_g. The shell of swept-up material has radius r_s and mass m_s per steradian. The time evolution of r_s is governed by the conservation of momentum:

$$\frac{d}{dt}(m_s V_s) = P_p r_s^2 , \tag{A1}$$

where P_p is the dynamic pressure exerted by the PN outflow.

If we make the simplifying assumptions (to be justified later) that $V_p \gg V_g$, and that the contribution to m_s is primarily from the swept-up wind of the red giant, then $P_p \simeq A_p r_s^{-2} V_p^2$, and equation (A1) may be solved for the (constant) velocity V_s, yielding

$$V_s = V_g\left[\frac{1}{2} + \sqrt{\frac{1}{4} + \left(\frac{V_a}{V_g}\right)^2}\right], \tag{A2}$$

where

$$V_a = V_p\sqrt{A_p/A_g} \tag{A3}$$

and V_a is the velocity of the shell when $V_g = 0$.

The quantity V_s may be estimated by assuming that the current position of the shell is the light echo region (i.e., $r_s = r_c$), and from the age of the PN t_o. Setting $r_c = 1.4$ pc and $t_o = 10^5$ yr (see § IV*f*) yields $V_s = 14$ km s^{-1}. This figure is comparable to the velocity of a red giant wind, and so $V_s \simeq V_g$. However, V_s must exceed V_g in order to produce a significant density enhancement at the shell radius r_c. It cannot exceed V_g by as much as an order of magnitude, however without conflicting with the age of the PN. Thus, from equation (A2), we find $V_s \simeq V_g \simeq V_a \simeq 10$ km s^{-1}. From the parameters for the light echo model discussed in § IV*e*, we estimate that the mass of dust per steradian in the slab is about $10^{-3}\ M_\odot$, yielding $m_s \simeq 10^{-1}\ M_\odot$ sr^{-1} if the dust/gas ratio is 10^{-2}. If this is identified with the mass of material swept up then $m_s = A_g r_c$, which leads to $A_g = 4.8 \times 10^{13}$ g cm^{-1}. If $V_g = 10$ km s^{-1}, the corresponding mass-loss rate is $9.0 \times 10^{-6}\ M_\odot$ yr^{-1}, plausible for a Mira variable. In addition, we have $A_p = 1.1 \times 10^{11}$ g cm^{-1} from the analysis of the adiabatic shock (§ IV*d*), so that equation (A3) yields $V_p \simeq 20 \times V_a \simeq 20 \times V_g$, or about 200 km s^{-1}. This velocity is consistent with the simplifying assumptions made above.

This picture, though not unique, is a self-consistent one provided a residual polar outflow occurs, continuous over most of the time since the onset of the PN phase. The velocity of this wind is about 200 km s^{-1}, and the mass-loss rate would be of order $10^{-7}\ M_\odot$ yr^{-1}.

REFERENCES

Allen, C. W. 1976, *Astrophysical Quantities* (London: Athlone).
Baars, J. W. M., Genzel, R., Pauliny-Toth, I. I. K., and Witzel, A. 1977, *Astr. Ap.*, **61**, 99.
Balick, B. 1987, in *Late Stages of Stellar Evolution*, ed. S. Kwok and S. R. Pottasch (Dordrecht: Reidel), p. 413.
Barlow, M. 1987, private communication.
Bath, G. T. 1978, *Quart. J.R.A.S.*, **19**, 442.
Becker, R. H., and Marshall, F. E. 1981, *Ap. J. (Letters)*, **244**, L93.
Beichman, C. A., Neugebauer, G., Habing, H. J., Clegg, P. E., and Chester, T. J., ed. 1985, *IRAS Explanatory Supplement* (JPL D-1855).
Bianchini, A., Hamzaoglu, E., and Sabbadin, F. 1981, *Astr. Ap.*, **99**, 392.
Bianchini, A., and Sabbadin, F. 1983, *Astr. Ap.*, **125**, 112.
Bode, M. F., and Evans, A. 1980, *Astr. Ap.*, **89**, 158.
Bode, M. F., Seaquist, E. R., and Evans, A. 1987, *M.N.R.A.S.*, **228**, 217.
Bode, M. F., Seaquist, E. R., Frail, D. A., Roberts, J. A., Whittet, D. C. B., Evans, A., and Albinson, J. S. 1987, *Nature*, **329**, 519.

Bond, H. E., Liller, W., and Mannery, E. J. 1978, *Ap. J.*, **223**, 252.
Burn, B. J. 1966, *M.N.R.A.S.*, **133**, 67.
Chevalier, R. A. 1977*a*, *Ann. Rev. Astr. Ap.*, **15**, 175.
———. 1977*b*, *Astr. Ap.*, **59**, 289.
Cordova, F. A., and Mason, K. O. 1984, *M.N.R.A.S.*, **206**, 890.
Couderc, P. 1939, *Ann. d'Ap.*, **2**, 271.
Cox, D. P., and Raymond, J. C. 1985, *Ap. J.*, **298**, 651.
Crampton, D., Cowley, A. P., and Fisher, W. A. 1986, *Ap. J.*, **300**, 788.
de Vries, C. P., and Le Poole, R. S. 1985, *Astr. Ap.*, **145**, L7.
Dickel, J. R., Eilek, J. A., and Jones, E. M. 1988, in *IAU Colloquium 101, Supernova Remnants and the Interstellar Medium*, ed. R. S. Roger and T. L. Landecker (Cambridge: Cambridge University Press), p. 235.
Draine, B. T. 1985, *Ap. J. Suppl.*, **57**, 587.
Draine, B. T., and Lee, H. M. 1984, *Ap. J.*, **285**, 89.
Duerbeck, H. W. 1981, *Pub. A.S.P.*, **93**, 165.
———. 1987*a*, private communication.
———. 1987*b*, *Space Sci. Rev.*, **45**, 1.
Fairclough, J. H., and Cooke, J. J. 1986, *Starlink User Note 70.7*, Rutherford and Appleton Labs.
Gallagher, J. S., and Starrfield, S. 1978, *Ann. Rev. Astr. Ap.*, **16**, 171.
Geiseking, F., Hippelein, H., and Weinberger, R. 1986, *Astr. Ap.*, **156**, 101.
Grauer, A. D., and Bond, H. E. 1983, *Ap. J.*, **271**, 259.
Gull, S. F. 1975, *M.N.R.A.S.*, **171**, 263.
Habing, H. 1988, in *Comets to Cosmology, Proc. 3rd IRAS Conf.*, ed. A. Lawrence (Berlin: Springer-Verlag), p. 81.
Heiles, C. 1976, *Ap. J.*, **204**, 379.
Hessman, F. V. 1987, private communication.
———. 1988, *M.N.R.A.S.*, submitted.
Hirst, C. J., and Cudlip, W. 1984, *Starlink User Note 60.1*, Rutherford and Appleton Labs.
Högbom, J. 1974, *Astr. Ap. Suppl.*, **15**, 417.
Hughes, D. H., Appleton, P. N., and Schombert, J. M. 1988, in preparation.
Iben, I., and Tutukov, A. V. 1984, *Ap. J.*, **282**, 615.
Jones, E. W., Smith, B. H., and Straka, W. C. 1981, *Ap. J.*, **249**, 185.
Kaplan, S. A. 1966, *Interstellar Gas Dynamics*, ed. F. D. Kahn (2d. ed.; NY: Pergamon Press).
Killean, N. E. B., Bicknell, G. V., and Ekers, R. D. 1986, *Ap. J.*, **302**, 306.
King, A. R. 1988, in *Classical Novae*, ed. M. F. Bode and A. Evans (NY: Wiley), in press.
Kopff, A. 1906, *Pub. Ap. Inst. Königstuhl-Heidelberg*, Vol. 2, No. 9.
Kulsrud, R. M., Bernstein, I. B., Kruskal, M., Fanucci, J., and Ness, N. 1965, *Ap. J.*, **142**, 491.
Livio, M., and Soker, N. 1988, *Ap. J.*, **329**, 764.
Low, F. J., *et al.* 1984, *Ap. J. (Letters)*, **278**, L19.
McLaughlin, D. B. 1960, in *Stars and Stellar Systems*, Vol. **6**, ed. J. L. Greenstein (Chicago: University of Chigaco Press), p. 585.
Meyer, F., and Meyer-Hoffmeister, E. 1979, *Astr. Ap.*, **78**, 167.
Miley, G. 1980, *Ann. Rev. Astr. Ap.*, **18**, 165.
Milne, D. K. 1987, *Australian J. Phys.*, **40**, 771.
Neugebauer, G., *et al.* 1984, *Ap. J. (Letters)*, **278**, L1.
Oort, J. H. 1951, in *Problems of Cosmical Aerodynamics*, ed. J. Burgess (Dayton, Ohio: Central Air Documents), p. 118.
Pacholczyk, A. G. 1970, *Radio Astrophysics* (San Francisco: Freeman).
Paczyński, B. 1971, *Acta Astr.*, **21**, 4.
Patterson, J. 1984, *Ap. J. Suppl.*, **54**, 443.
Payne-Gaposchkin, C. 1957, *Galactic Novae* (Amsterdam: North-Holland).
Perrine, C. D. 1902, *Ap. J.*, **14**, 249.
Pottasch, S. R. 1959, *Ann. d'Ap.*, **22**, 412.
———. 1980, *Astr. Ap.*, **89**, 336.
Raymond, J. C., Cox, D. P., and Smith, B. W. 1976, *Ap. J.*, **204**, 290.
Razin, V. A. 1960, *Radiofizika*, **3**, 584.
Reynolds, S. P. 1988, in *Galactic and Extragalactic Radio Astronomy*, ed. G. L. Verschuur and K. I. Kellermann (New York: Springer).
Reynolds, S. P., and Chevalier, R. A. 1984, *Ap. J. (Letters)*, **281**, L33.
Ritchie, G. W. 1901, *Ap. J.*, **14**, 293.
Ritter, H. 1976, *M.N.R.A.S.*, **175**, 279.
Roberts, J. A. 1989, Ph.D. thesis, Lancashire Polytechnic.
Roberts, J. A., Bode, M. F., Lopez, J. A., Ecchevarria, J. L., and Whittet, D. C. B. 1988, in preparation.
Sabbadin, F., and Bianchini, A. 1983, *Astr. Ap. Suppl.*, **54**, 393.
Sabbadin, F., Gratton, R. G., Bianchini, A., and Ortolani, S. 1984, *Astr. Ap.*, **136**, 181.
Savage, B. D., and Mathis, J. S. 1979, *Ann. Rev. Astr. Ap.*, **17**, 73.
Schaefer, B. 1988, *Ap. J.*, **327**, 347.
Schlickeiser, R. 1986, in *Cosmic Radiation in Contemporary Astrophysics*, ed. M. M. Shapiro (Dordrecht: Reidel), p. 27.
Schweizer, E., Mattei, J., and Hurst, G. M. 1986, *IAU Circ.*, No. 4274.
Seaquist, E. R. 1989, in *Classical Novae*, ed. M. F. Bode and A. Evans (Chichester: Wiley), p. 143.
Seaquist, E. R., Frail, D. A., Bode, M. F., Roberts, J. A., Whittet, D. C. B., Evans, A., and Albinson, J. S. 1988, in *IAU Colloquium 101, The Interaction of Supernova Remnants with the Interstellar Medium* (Cambridge: Cambridge University Press), p. 47.
Seitter, W. C. 1985, in *Production and Evolution of the Chemical Elements*, ed. I. J. Danziger, *et al.* (Garching: ESO), p. 253.
Seitter, W. C., and Duerbeck, H. W. 1987, in *RS Ophiuchi (1985) and the Recurrent Nova Phenomenon*, ed. M. F. Bodel (Utrecht: VNU Sci Press), p. 71.
Sofue, Y., and Fujimoto, M. 1983, *Ap. J.*, **265**, 722.
Stewart, B. 1987, *Starlink User Note 90.1*, Rutherford and Appleton Labs.
Swope, H. 1940, *Harvard Bull.*, No. 913, 11.
Takakara, F. 1986, in *Plasma Astrophysics*, ed. T. D. Guyenne and L. M. Zeleny (ESA SP-251), p. 253.
van den Bergh, S. 1971, *Pub. A.S.P.*, **83**, 819.
———. 1977, *Pub. A.S.P.*, **89**, 637.
von Küstner, F. 1921, *Astr. Hachr., Jubilamsnummer*, p. 18.
Watson, M. G., King, A. R., and Osborne, J. 1985, *M.N.R.A.S.*, **212**, 917.
Weaver, H., and Williams, D. R. W. 1973, *Astr. Ap. Suppl.*, **8**, 1.
Webbink, R. 1985, in *Interacting Binary Stars*, ed. J. E. Pringle and R. A. Wade (Cambridge: Cambridge University Press), p. 39.
Weiland, J. L., Blitz, L., Dwek, E., Hauser, M. G., Magnani, L., and Rickard, L. J 1986, *Ap. J. (Letters)*, **306**, L101.
Williams, R. E. 1981, *Sci. Am.*, **244**, 96.
———. 1987, private communication.
Wu, C. C., Panek, R. J., Holm, A. V., Raymond, J. C., Hartmann, L. W., and Swank, J. H. 1989, *Ap. J.*, **339**, 443.
Zelick, M. 1977, *Ap. J.*, **218**, 118.

J. S. ALBINSON and A. EVANS: Department of Physics, University of Keele, Staffordshire, England ST5 5BG, UK

M. F. BODE and J. A. ROBERTS: School of Physics and Astronomy, Lancashire Polytechnic, Corporation Street, Preston, England PR1 2TQ, UK

D. A. FRAIL and E. R. SEAQUIST: Department of Astronomy, University of Toronto, Toronto, Ontario, Canada, M5S 1A7